Coprecipitation of curcumin/PVP with enhanced dissolution properties by the supercritical antisolvent process

Lessa Matos, Ravenna; Lu, Tiejun; Prosapio, Valentina; McConville, Christopher; Leeke, Gary; Ingram, Andrew

DOI:
10.1016/j.jcou.2019.01.005

Coprecipitation of curcumin/PVP with enhanced dissolution properties by the supercritical antisolvent process

Ravenna Lessa Matos[a,*], Tiejun Lu[a], Valentina Prosapio[a], Christopher McConville[b], Gary Leeke[c], Andrew Ingram[a]

[a]Centre for Formulation Engineering, School of Chemical Engineering, University of Birmingham, Birmingham, B15 2TT, UK

[b]School of Pharmacy, Institute of Clinical Sciences, Sir Robert Aitken Institute for Medical Research, University of Birmingham, Birmingham, B15 2TT, UK

[c]Centre for Bioenergy & Resource Management, Cranfield University, Cranfield, MK43 0AL, UK

* RXL523@student.bham.ac.uk

ABSTRACT

The poor solubility of curcumin (CURC) in aqueous media leads to a low bioavailability, which prevents its application in pharmaceutical formulations. In this work, the Supercritical Antisolvent process (SAS) was used to produce coprecipitates of CURC and poly (vinyl pyrrolidone) (PVP) from mixtures of ethanol and acetone. The effects of operating parameters: pressure, temperature, solution concentration, drug/polymer mass ratio and solution flow rate were analysed for a 70-30 (v/v) acetone-ethanol mixture. It was found that the composition of acetone in the solvent mixture is the parameter that affects particle size and curcumin recovery the most. The thermal behaviour, crystallinity, molecular interactions, apparent solubility, release profile of the coprecipitates and possible degradation of curcumin were investigated. The results showed that the SAS process is effective in preparing amorphous formulations of CURC/PVP with an apparent solubility of more than 600 times higher than that of the physical mixture of the raw compounds.

Keywords: coprecipitation; curcumin; PVP; supercritical antisolvent process; dissolution

1. Introduction

Curcumin (CURC) is a polyphenolic hydrophobic compound extracted from the roots of *Curcuma longa* and traditionally used as a spice and food additive. It has been demonstrated that curcumin has

a wide range of therapeutic properties such as anticancer, antioxidant, antimicrobial and anti-inflammatory [1,2]. However, the use of curcumin in drug formulations is still not approved by the Food and Drug Administration (FDA), limited by several reasons including its low oral bioavailability caused by its poor solubility in aqueous media, low absorption and fast intestinal metabolism. In addition, curcumin undergoes degradation under light, heat and alkaline pH [3,4].

In recent decades, several curcumin formulations have been developed to address these issues including nanoparticles, liposomes, polymeric micelles, dendrimers and hydrogels [5–7]. The coprecipitation of active pharmaceutical ingredients (API) with hydrophilic polymers is advantageous because it can improve the API dissolution properties while protecting it against degradation. Poly(vinyl pyrrolidone) (PVP) was selected in this work because it is a biodegradable polymer approved as an inactive ingredient by the FDA and hence widely used in pharmaceutical applications. Several studies have demonstrated its ability in modifying the crystallisation kinetics of poorly water-soluble compounds by producing amorphous formulations with improved dissolution profile [8–10]. PVP is also expected to inhibit drug recrystallisation in the gastro-intestinal tract after oral administration [11,12], giving time for drug molecules to be absorbed into the systemic circulation, thus increasing its bioavailability [13].

The preparation of solid dispersions of curcumin and PVP with different molecular weights has been reported using conventional micronization techniques, such as spray drying [14] and solvent evaporation [15–17]. These methods have disadvantages such as the use of high temperature, which causes the degradation of thermo-sensitive compounds, low yields and high residual solvent content in the formulation, often requiring an extra processing step. Moreover, the control of particle morphology, particle size and size distribution is difficult [18–20]. In smaller quantities, PVP has been used as a stabilizer for curcumin nanoparticles prepared via liquid antisolvent methods followed by freeze drying [21–23].

Supercritical fluids (SCFs) are attractive for particle precipitation as they combine liquid-like properties, such as high solvation power, and gas-like properties, including high diffusivity and compressibility. SCF-based micronization has demonstrated advantages over conventional techniques

since particle size can be controlled through the manipulation of the operating parameters, the use of relatively low temperatures and formulations with low or no residual solvent can be obtained [24,25]. Carbon dioxide is a usual choice for SCF-based micronization processes since it is inexpensive, non-toxic, non-flammable, environmentally benign and it has a relatively low critical pressure (7.39 MPa) and critical temperature (31.1°C). Depending on the role played by the supercritical carbon dioxide (sc-CO_2) in relation to the solute, it can act as solvent, co-solute, antisolvent, dispersing agent, plasticizer or reaction medium.

In the Supercritical Antisolvent (SAS) process, the solute is typically dissolved in an organic solvent and then sprayed into a high pressure vessel through which sc-CO_2 is passed continuously. The instantaneous diffusion of sc-CO_2 into the liquid solution and, in minor extent, the evaporation of the liquid to the supercritical phase leads to the supersaturation of the liquid solution and precipitation of the solute, which is collected on a filter. Solvent and antisolvent are then separated via simple depressurization in a separator located downstream the precipitation vessel [26]. Although studied for many years, the SAS process is still not widely used in the pharmaceutical industry. A deeper understanding of the phenomena involved in each step is required to allow the selection of the most appropriate operating conditions and enable process control. Extensive use of SAS at industrial scale to process pharmaceutical and food ingredients is believed likely in the future, especially due to the need of finding more environmentally friendly technologies as recently discussed [27]. A key feature of SAS is its ability to process a wide variety of compounds to obtain several morphologies and sizes including crystals, nanoparticles, microparticles and expanded microparticles [28–30]. However, the use of SAS to produce coprecipitates has not always been successful. In some works, irregular and coalescing particles with wide particle size distribution [31] and low encapsulation efficiency [32] were obtained and the demonstration of an effective coprecipitation through the improvement of the drug dissolution properties is hardly reported [33].

In our recent work, curcumin was simultaneously precipitated and coated on the surface of lactose particles by the integration of the SAS process with a fluidized bed under pressure (SAS-FB) to improve the flow properties of the formulation [25]. In this work, the aim is to improve also the

dissolution properties of curcumin through its coprecipitation with PVP by SAS, which is a suitable technique to treat thermo- and light-sensitive compounds, since low temperatures can be used and the experiments are carried out away from light.

Other SCF-assisted processes have been used to produce CURC/PVP coprecipitates. Adami et al. [34] obtained spherical and collapsed particles with mean size ranging from 220 - 380 nm by the supercritical assisted atomization (SAA), using ethanol as solvent. The issue here is the use of high temperature (80 °C) since curcumin degradation is known to be intensified above 60˚C [4,35]. The quantification of product recovery and possible degradation of curcumin were not presented by the authors. The atomized rapid injection solvent extraction (ARISE) method has also been applied for the coprecipitation of curcumin in ternary composites with PVP and cyclodextrins, with very few experiments being carried out with the binary CURC/PVP. As the intended application was pulmonary delivery, microparticles were produced and in some of the images presented it was possible to distinguish curcumin crystals in a porous structure, which indicate that the materials precipitated separately [36–38]. Although there are similarities between the SAS and ARISE processes in terms of the role of sc-CO_2, differences between the mixing mechanism can lead to different results. The use of SAS process to produce CURC/PVP coprecipitates for pharmaceutical application has been reported once by Chhouk et al. [39]. They used a micro-swirl mixer, a patented device, to process curcumin and PVP from a 90-10 acetone-ethanol mixture. Highly coalescing nanoparticles (25 - 342 nm) were obtained while very relevant information such as total product recovery, curcumin recovery and drug dissolution kinetics was not presented. Only samples with low curcumin content (3-9%) were produced and no explanation was given for the selection of the solvent mixture used.

Therefore, it is clear that a deeper study and understanding of the coprecipitation of curcumin and PVP by SAS is necessary, which is the aim of this work. We also want to test if it is possible to obtain non-coalescing nanoparticles of the composite material, with high curcumin content (up to 25%) and improved dissolution properties, without the aid of a complex mixing device, as reported in the aforementioned work [39]. For the first time, different organic solvent mixtures were studied to

understand how adjusting the solvent properties (solvation power) can modulate particle size and recovery of CURC/PVP coprecipitates. The effects of operating parameters, pressure, temperature, initial solution concentration, drug/polymer ratio and solution flow rate, were also investigated.

2. Experimental

2.1. Materials

Curcumin (CURC, purity ≥ 90%) was purchased from Cayman Chemical and poly (vinyl pyrrolidone) (PVP, Mw = 10 kg/mol), sodium dodecyl sulphate (SDS) and acetic acid (glacial class 8, purity ≥ 99%) were purchased from Sigma Aldrich, UK and Ireland. Ethanol (EtOH, purity = 99.97%) and carbon dioxide (purity ≥ 99.8%) were purchased from VWR Chemicals and BOC, UK, respectively. Acetone (Ac, purity = 99.99%) and acetonitrile (purity = 99.99%) were purchased from Fisher Chemical, UK. All materials were used as-received.

2.2. SAS equipment

Fig. 1 shows the diagram of the SAS process. CO_2 is delivered to the precipitator or high pressure vessel (HPV) by an air driven pump (PowerStar 4; Model: P464, Sprague). Before entering the pump, the CO_2 line passes through a cold bath (Grant C1G) operated below 0°C to promote the condensation of CO_2 and avoid pump cavitation. After the pump, the CO_2 is heated in a hot water bath (Tecam open bath TECAM1 + Grant Type ZA Grant bridge control unit) to achieve the desired operating temperature and then it enters the precipitation vessel via a tube of 1/4 inch OD. The solvent/solution is delivered by an HPLC pump (Waters M-6000). Detail of the precipitation vessel and injection device can be seen in the supplementary material. A stainless steel capillary with internal diameter of 100 µm, external diameter of 1/32 in and 20 cm in length (Thames Restek UK), placed concentric with the CO_2 delivery tube, is used as a nozzle to promote the atomization of the solvent/solution,. The nozzle end, where the solution is sprayed out, is placed 2.4 mm lower than the end of CO_2 inlet tube to avoid the partial blockage of the CO_2 tube with polymer as observed in some preliminary experiments.

The high pressure vessel (HPV) used as precipitator is a 500 ml cylindrical jacketed autoclave (Baskerville Scientific, UK) containing three saphire windows. Hot water is continuously supplied to the heating jacket to keep the HPV at the desired operating temperature by the same heat exchanger used to heat up the CO_2 line. The precise reading of the temperature and pressure inside the vessel is enabled by a thermocouple (RS PRO Type K) and pressure transducer (GE Druck PTX 1400) displayed in a digital process indicator (GE Druck DPI 282). The HPV is protected against overpressure by a safety valve (Swagelok SS-4R3A). Precipitated particles are collected by a cellulose thimble (43 mm x 123 mm, Whatman) installed inside the HPV, allowing the flow of CO_2 + organic solvent mixture. The chamber pressure is controlled by a pressure regulator (Tescom 26-1752-24) located in the by-pass of the CO_2 pump. A middle pressure vessel (MPV) of approximately 300 ml (Swagelok double-ended sample cylinder, 316L-HDF4-300-PD) is connected to the precipitator through a micrommetric valve (MMV) (Hoke 1335G4Y), which enables the manual control of the CO_2 flow rate, which is displyed by a mass flow transmitter (Rheonik RHE08) placed in the CO_2 inlet to the HPV. The MPV pressure is controlled by a pressure reducing regulator (GO BP3-1A11I5J114) at around 1 MPa. It is also protected against overpressure by a safety valve (Swagelok SS-4R3A). Due to the pressure drop, the MPV enables the separation of the phases: the organic solution is condensed and collected in bottom of the vessel, while gaseous CO_2 flows out from the top. The CO_2 then passes through the pressure reducing regulator, decreases its pressure to ambient, enters a cyclone to remove fine droplets of solution possibly entrained in the gas phase and is finally directed to vent. A third heat exchanger and pump (Tecam circulator C-400) supply hot water through a flexible pipe which surrounds the MMV and MPV to avoid their freezing due to depressurization. Additional manometers (Budenberg 966GP) are placed in the outlet of the CO_2 cylinder, outlet of the CO_2 pump, inlet of the precipitation vessel and inlet of the MPV.

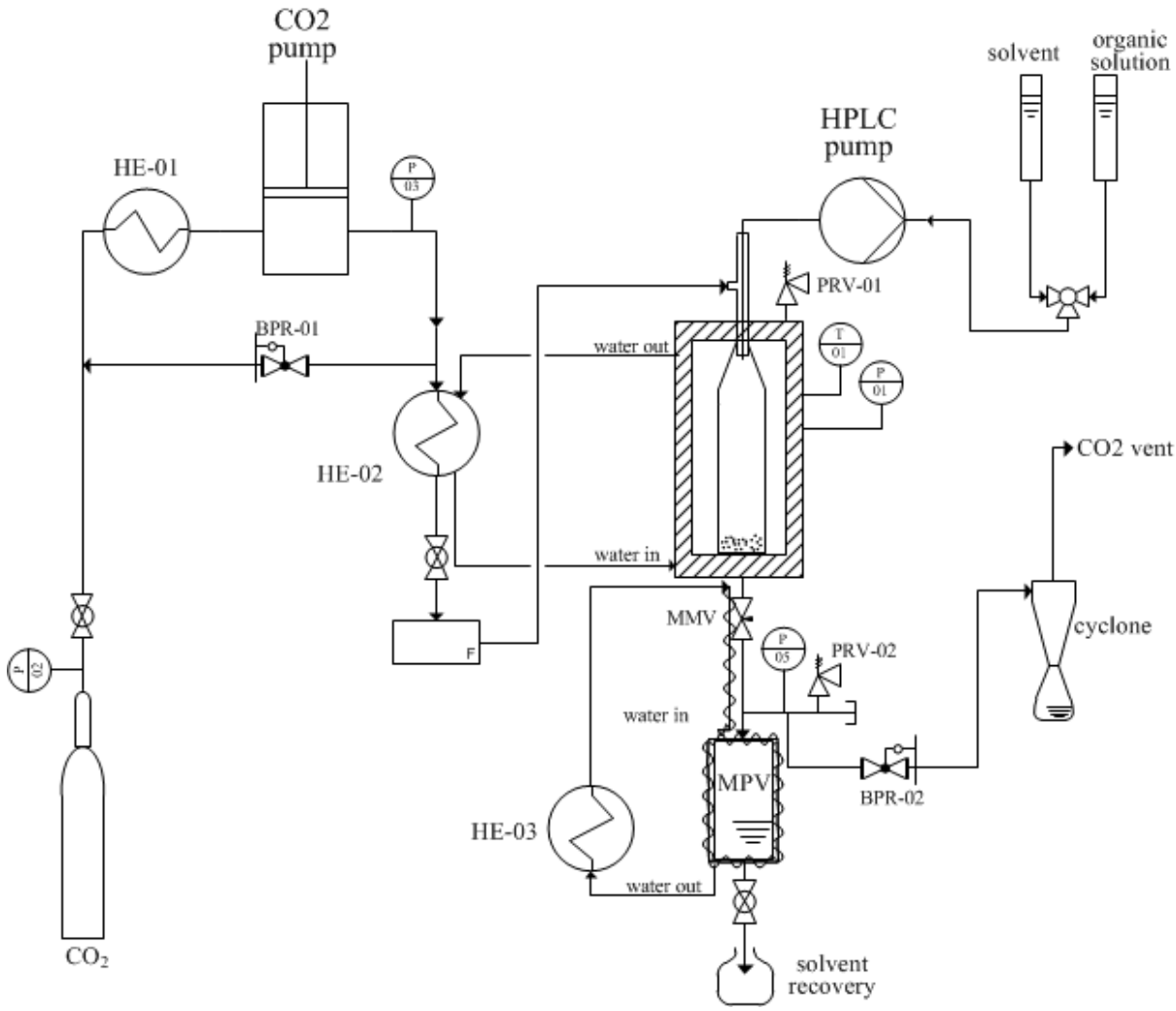

Fig. 1. SAS experimental setup.

2.3. SAS experimental procedure

Firstly, the precipitator is pressurized with CO_2 until the desired pressure is achieved. At this point, the outlet micrometric valve (MMV) is opened to give a constant flow of sc-CO_2 (40 g/min for all experiments), whilst maintaining pressure (**Fig. 1**).

Solvent is then pumped into the precipitator through the 100 µm capillary nozzle for enough time to reach quasi-steady state composition of solvent and CO_2, before the pump is switched to a solution of curcumin, PVP or curcumin and PVP. As the precipitation happens inside of the cellulose thimble and glass connector (dimensions shown in the supplementary material), rather than in the whole volume of the vessel, the mean residence time of the materials varies between 2 and 5 minutes, being close to 3 minutes at 40°C and 9.0 MPa. Assuming the behaviour of an ideal stirred tank, at least three residence

times of CO_2 and solvent were allowed to flow before the drug solution was injected so the CO_2/solvent ratio in the vessel was at least 95% of the inlet composition.

After the desired amount of curcumin and/or PVP has been injected into the precipitator (usually 400 mg of solute in 40 ml of solution), the pump is reverted to solvent to purge the line (10 ml) and assure all the solution inside the dead volume has been delivered. Then the solvent pump is stopped and fresh CO_2 runs through the system to remove any residual solvent. Finally, the pressure is gradually decreased to ambient, the thimble is removed from inside the high pressure vessel and then the powder is collected with a spatula. Some material remains entrapped in the pores of the thimble and therefore most, but not all, precipitated powder can be collected. No powder is found outside the thimble or inside the vessel, however possible loss of nanoparticles might occur in the first minutes of particle generation but it should stop as soon as the particles build up a filter cake.

2.4. Preparation of the physical mixture

Physical mixtures (PM) of curcumin (CURC) and PVP, obtained by shaking the powders in sealed vials for 5 minutes, were prepared with mass ratios of 1:3 and 1:10 CURC/PVP for comparison with equivalent SAS coprecipitated samples.

2.5. Analyses

2.5.1. Scanning electron microscopy (SEM)

Scanning Electron Microscopy (SEM - model Philips XL-30 FEG) was used to observe the morphology and particle size of raw materials and coprecipitates at 10 kV and 10 mA. Samples were initially fixed on a double-sided adhesive carbon tape and sputter coated (Polaron SC 7640) with gold for 3 min at 25 mA. Image J analysis software was used to measure particle size and size distribution. Usually 500 particles of each sample in SEM images with different magnifications were accounted. The results are presented as mean diameter ± arithmetic standard deviation.

2.5.2. Total product recovery

The total product recovery (Rec.) is an important parameter to assess the efficiency of a process. It was defined as the percentage ratio of the final mass of precipitates collected to the initial mass delivered to the precipitator, as shown below:

$$Rec. = \frac{mass\ (CURC + PVP)\ collected}{mass\ (CURC + PVP) feed} \times 100\%$$

2.5.3. Curcumin content and recovery

Accurately weighed samples were dissolved in 50% v/v water-acetone solution and curcumin concentration was determined using an ultraviolet (UV)–visible spectrophotometer (Thermo Scientific Orion AquaMate) to measure the solution absorbance at λ = 425 nm. At this wavelength the absorbance of PVP is negligible (as reported in the supplementary material), while that of curcumin is proportional to its concentration (R^2 = 0.999). All the measurements were taken within few minutes of sample dissolution so the effect of curcumin degradation in contact with water can be considered negligible. Each sample was analysed 3-5 times and the mean values are reported. Curcumin content (Cont.) was obtained by dividing the mass of curcumin in the analysed sample by the total sample mass, as follows:

$$Cont. = \frac{CURC\ mass\ in\ sample}{total\ sample\ mass} \times 100\%$$

Curcumin recovery (CURC Rec.) was calculated as shown below:

$$CURC\ Rec. = \frac{Rec. \times Cont.}{CURC\ content\ in\ feed}$$

The use of the cellulose thimble described here very conveniently facilitates the recovery of the powder without requiring the precipitator to be completely disassembled from the rig and cleaned after each run. The amount of curcumin retained in the pores of the cellulose thimble (filter) was quantified by washing each filter with a known volume of 50% v/v water-acetone and analysing the solution by (UV)–visible spectrophotometer.

2.5.4. High Performance Liquid Chromatography (HPLC)

Raw curcumin and processed samples were analysed by HPLC to investigate possible degradation of curcumin after processing. A gradient elution was employed using an Accucore C18 column (30 mm x 2.1 mm, 2.6 µm, Thermo Scientific) starting with a mobile phase containing acetonitrile and 2% acetic acid initially at 10:90 (v/v). The proportion of the materials was gradually changed to 50:50 by 10 minutes with each run lasting 16 minutes in total. A flow rate of 0.85 mL/min, a column temperature of 30°C, a detection wavelength of 425 nm and an injection volume of 20 µL were employed [40]. Sample solutions were prepared in 50:50 acetonitrile-2% acetic acid and filtered with a 0.22 µm PTFE syringe filter prior to analyses.

2.5.5. X-ray diffraction (XRD)

Raw materials and coprecipitates were analysed by X-ray diffraction (XRD, Bruker D8, UK) at 40 kV and 30 mA to determine the degree of crystallinity before and after processing. Patterns were obtained with a beam angle varying from 5° to 40° and a step size of 0.023°.

2.5.6. Differential Scanning Calorimetry (DSC)

The thermal behaviour of the samples and unprocessed compounds were assessed by Differential Scanning Calorimetry (Discovery DSC 25, TA Instruments) working with a nitrogen purge of 50 ml/min. A heat-cool-heat cycle was employed to eliminate possible interference of moisture and relieve stress allowing a proper determination of the glass transition temperature (T_g) of the materials [41–43]. First, the samples were placed in aluminium pans and accurately weighed. A hole was made on each lid, allowing the removal of moisture with the purge gas. They were then heated from 50°C to 160°C (above the glass transition of PVP and below the melting point of curcumin) at 20°C/min and after that quench cooled (100°C/min) to the initial temperature. Finally, they were heated to 250°C at 20°C/min. The results presented correspond to the final heating stage in which the glass transition temperature, melting point and enthalpy of fusion were measured. TA Instruments Universal Analysis Software was used to estimate the glass transition temperature (T_g, midpoint of the change in heat capacity) and melting point (T_m, onset temperature) of the samples.

2.5.7. Fourier transform infrared spectroscopy (FTIR)

Fourier transform infrared spectroscopy (FTIR, Jasco-6300) equipped with an attenuated total reflectance (ATR) accessory was used to analyse the chemical structure of coprecipitates and possible molecular interactions generated after processing. 64 scans were taken in a range of 800-4000 cm^{-1} with a resolution of 4 cm^{-1} [44,45].

2.5.8. Drug apparent solubility

The apparent solubility of the materials was analysed by adding excess sample to 2 ml of distilled water and then sonicating the suspension at 25°C for 15 minutes. Then the suspension was filtered with a 0.22 µm PTFE syringe filter. Curcumin concentration was determined via UV–visible spectrophotometer. Experiments were performed in triplicates and the mean values are shown.

2.5.9. In vitro dissolution studies

In vitro dissolution studies were performed using a USP 2 dissolution apparatus (rotating paddles). Samples were accurately weighed with equivalent amount of curcumin (5 ppm) and incubated at 37 ± 0.5°C in 200 mL of water and 0.25% w/v sodium dodecyl sulphate (SDS). The rotation of the paddles was set to 100 rpm. 2 mL of the solution was withdrawn at different time intervals and replaced with the same volume of fresh medium. Curcumin concentration was then analysed by UV–visible spectrophotometer. Curcumin release was calculated as follows:

$$Release\ (\%) = \frac{m_t}{m_{100\%}} \times 100\%$$

where m_t represents the mass of curcumin released at time t and $m_{100\%}$ is the mass of curcumin at complete dissolution. The tests were performed in triplicates and the mean values are reported.

3. Results and discussion

In the SAS process, the selection of the operational conditions is crucial in the success of the precipitation [46,47]. Knowledge of thermodynamics, jet hydrodynamics, mass transfer and crystallization kinetics is required to properly understand the results. Supersaturation is the driving force for precipitation and can be defined as the ratio between the solute concentration in the solvent-

CO_2 system and the equilibrium concentration (solubility). Particle size is dependent on the degree of solution supersaturation achieved. High initial solution concentration and low equilibrium concentration of the solute in the fluid phase leads to high supersaturation. Additionally, the supersaturation can be affected by the flow rate of the materials used, responsible for the turbulence and mixing between the phases. The yield of precipitation is especially influenced by the concentration of solute present in the effluent solution [48–50].

For most experiments, pressure, temperature and CO_2 flow rate were kept constant at 40°C, 9.0 MPa and 40 g/min, giving a CO_2 molar fraction (X_{CO2}) between 0.98 - 0.99. According to the literature [51], these conditions would ensure that the precipitation happens in the supercritical region of the mixed solvent-CO_2.

3.1. Precipitation of single compounds

Prior to coprecipitation experiments, the compounds were processed separately to compare with their precipitation behaviour (morphology and size) when processed at the same conditions of the coprecipitates. This information is useful to evaluate the success of the coprecipitation and any possible changes in morphology that can occur when the two compounds are processed simultaneously.

PVP is a biocompatible polymer commonly used in drug delivery applications and has been previously precipitated by SAS [24,52,53]. In this work, the experiments were carried out initially using ethanol as solvent, solution concentration of 10 mg/ml and solution flow rate of 1 ml/min, resulting in a CO_2 molar ratio of $X_{CO2} = 0.98$.

Table 1 summarises the operational conditions and the results obtained. In run #1 a negligible amount of powder was recovered. Since PVP is highly soluble in ethanol [24], the concentration used might have not been high enough to achieve the minimum supersaturation required for particle generation. In an attempt to increase the supersaturation, in run #2, the solution concentration was increased to 20 mg/ml and the other parameters were kept constant; however this concentration was still not enough and the precipitation was again unsuccessful.

Another way to affect the supersaturation, while keeping the initial solution concentration constant, is by changing the solubility (equilibrium concentration) of the solute in the fluid phase. As the solubility of PVP in ethanol is much higher than in acetone (315 mg/ml versus 7 mg/ml), solvent mixtures of acetone-ethanol (Ac-EtOH) were used. As a consequence of the addition of a poor solvent to PVP (acetone), higher supersaturation levels can be achieved and a higher proportion of the solute precipitates, increasing product recovery. In fact, the addition of acetone into ethanol to produce a 50% v/v mixture allowed a successful precipitation in run #3 and the increase in acetone content to 90% v/v further improved PVP recovery in run #4 from 2.0 to 87.0% (**Table 1**). These results demonstrate the significant impact of changing the solute solubility in the fluid phase by the manipulation of the solvent power of the organic solution. Pure acetone was not used to process PVP since PVP solubility in acetone is below 10 mg/ml (approximately 7 mg/ml).

The precipitation of PVP from acetone-ethanol mixtures has been previously investigated. However, contrary to what has been demonstrated here, De Marco et al. [24] reported a process yield of around 90% for experiments with several acetone-ethanol mixture compositions, while Rossmann et al. [52] did not discuss product recovery. **Fig. 2**a,b shows the comparison between raw and processed PVP obtained from run #4. It is clear that there is a decrease in particle size and a narrowing of the particle size distribution after SAS processing.

Curcumin was then processed at the same conditions used for PVP. The solubility of curcumin in acetone was estimated to be around 58 mg/ml, while in ethanol it was below 5 mg/ml. In the experiment with pure ethanol (run #5), a concentration of 2 mg/ml was used; however no powder could be recovered. When curcumin was processed by a 50-50 Ac-EtOH solution (run #6) and by pure acetone (run #7) at 10 mg/ml, product recovery was 23.4% and 34.8%. Despite the higher initial saturation of the ethanol solution in comparison to the acetone solution, when CO_2 is present in the system a co-solvent effect seems to be taking place with ethanol, as already observed for other systems [54,55]. This explains the lower product recovery when ethanol was used. The lower recovery of curcumin produced by similar processes from alcoholic solutions compared to acetone have also been observed elsewhere [56]. The authors explained that the higher volume expansion and

consequently more efficient reduction in solvent power are achieved in the case of acetone possibly leading to higher recovery. In runs #5, #6 and #7, the amount of curcumin retained in the filter decreased from 56.4% to 48.2% and 33.0%, respectively (**Table 1**). **Fig. 2**c shows rod-like crystals of raw curcumin with a wide size distribution, while curcumin processed by a 50% Ac-EtOH (**Fig. 2**d, run #6) and by pure acetone (**Fig. 2**e, run #7) has an irregular morphology with smaller dimensions. In **Fig. 2** it is also possible to see that PVP and curcumin precipitate in completely different morphologies when processed at the same conditions. This underlines the complexity of the SAS process and its compound-dependent characteristic.

#	*p* (MPa)	T (°C)	f (ml/min)	C_{TOT} (mg/ml)	Solvent	Solvent volumetric composition Ac-EtOH	drug/polymer mass ratio	Total product recovery (%)	Curcumin recovery (%)	Curcumin retained in the filter (%)	m.d. (nm)	s.d. (nm)	Morphology
1	9.0	40	1	10	EtOH	0-100	pure PVP	≈ 0	-	-	-	-	-
2	9.0	40	1	20	EtOH	0-100	pure PVP	≈ 0	-	-	-	-	-
3	9.0	40	1	10	Ac-EtOH	50-50	pure PVP	2.0	-	-	-	-	-
4	9.0	40	1	10	Ac-EtOH	90-10	pure PVP	87.0	-	-	123	27	SMP
5	9.0	40	1	2	EtOH	0-100	pure curcumin	≈ 0	≈ 0	56.4	-	-	-
6	9.0	40	1	10	Ac-EtOH	50-50	pure curcumin	23.4	23.4	48.2	-	-	-
7	9.0	40	1	10	Acetone	100-0	pure curcumin	34.8	34.8	33.0	-	-	Irregular
8	9.0	40	1	10	EtOH	0-100	1:3	43.1	45.5	41.4	-	-	Irregular
9	12.0	40	1	10	EtOH	0-100	1:3	63.1	68.1	25.5	-	-	Irregular
10	9.0	40	1	10	Ac-EtOH	10-90	1:3	58.0	65.3	29.3	327	102	SMP
11	9.0	40	1	10	Ac-EtOH	30-70	1:3	74.3	76.6	10.2	177	57	SMP
12	9.0	40	1	10	Ac-EtOH	50-50	1:3	77.6	78.6	6.7	135	36	SMP
13	9.0	40	1	10	Ac-EtOH	70-30	1:3	87.1	89.0	2.5	96	25	NP
14	9.0	40	1	10	Ac-EtOH	90-10	1:3	90.0	89.2	0.8	51	12	NP
15	8.0	40	1	10	Ac-EtOH	70-30	1:3	56.4	59.6	20.8	181	48	SMP
16	12.0	40	1	10	Ac-EtOH	70-30	1:3	79.1	88.1	6.7	67	17	NP
17	9.0	35	1	10	Ac-EtOH	70-30	1:3	89.5	94.9	5.0	72	20	NP
18	9.0	50	1	10	Ac-EtOH	70-30	1:3	76.9	83.7	9.9	176	56	SMP
19	9.0	40	1	5	Ac-EtOH	70-30	1:3	80.7	88.9	5.6	65	14	NP
20	9.0	40	1	20	Ac-EtOH	70-30	1:3	80.2	90.5	6.2	117	30	SMP
21	9.0	40	1	10	Ac-EtOH	50-50	1:10	60.7	60.2	26.3	-	-	CM
22	9.0	40	1	10	Ac-EtOH	70-30	1:10	79.7	79.9	5.5	173	76	SMP
23	9.0	40	1	10	Ac-EtOH	70-30	1:20	69.2	67.9	9.6	205	49	SMP
24	9.0	40	0.5	10	EtOH	0-100	1:10	34.3	36.1	48.7	-	-	CM
25	9.0	40	0.5	10	Ac-EtOH	10-90	1:10	47.6	50.8	24.9	-	-	CM
26	9.0	40	0.5	10	Ac-EtOH	70-30	1:10	79.7	82.3	4.0	220	85	SMP

Table 1. Experimental conditions and results (*p* = pressure; f = solution flow rate; C_{TOT} = total solute concentration; m.d.: mean diameter; s.d.: standard deviation; SMP: sub-microparticles; NP:

nanoparticles; CM: coalescing material). Experiments performed at 40°C and CO_2 flow rate of 40 g/min.

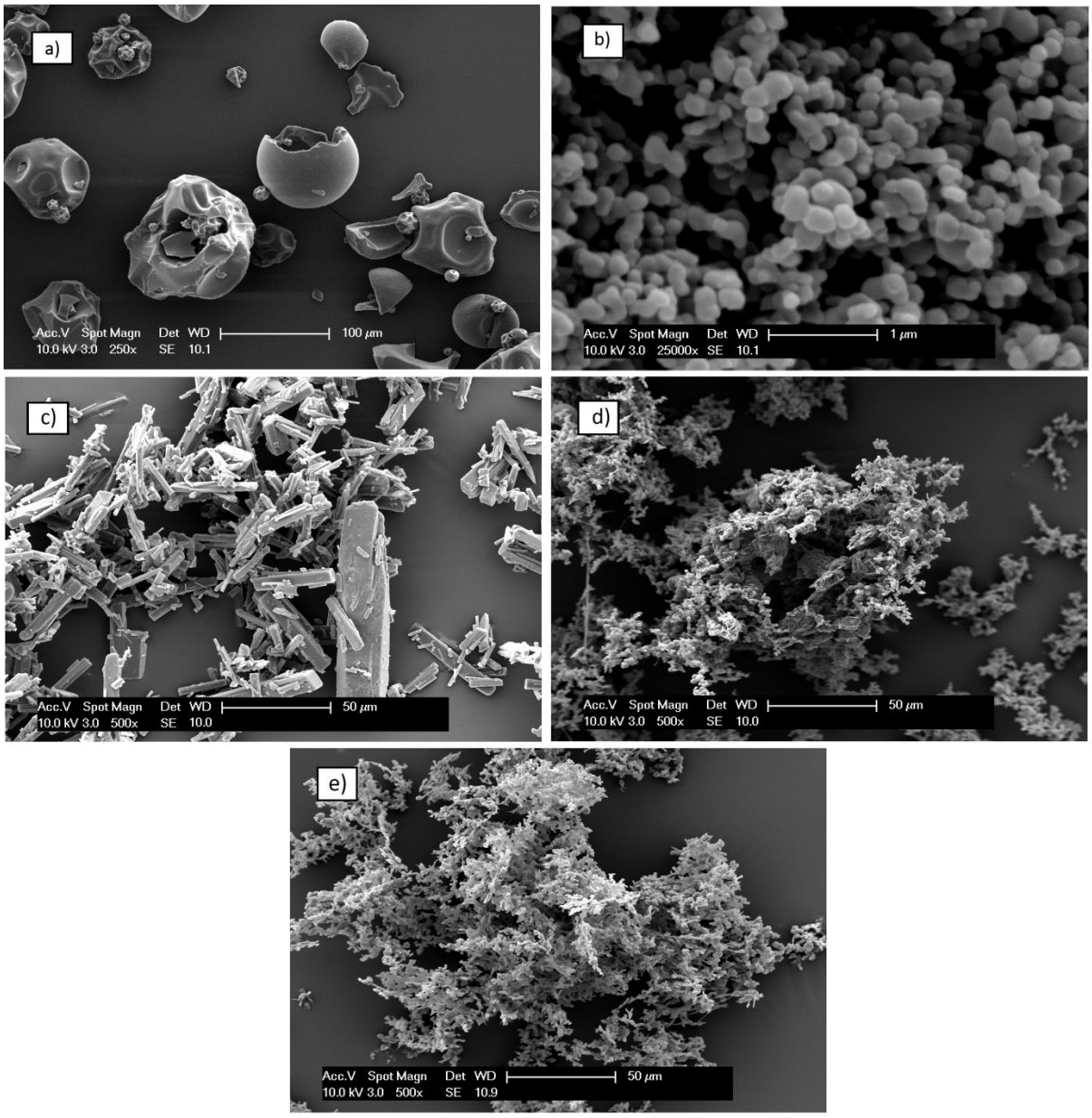

Fig. 2. SEM images of: a) raw PVP; b) PVP processed by SAS (run #4); c) raw curcumin; d) curcumin processed by SAS from 50% Ac-EtOH (run #6); e) curcumin processed by SAS from acetone (run #7).

3.2. Coprecipitation of CURC/PVP

It has been demonstrated elsewhere that PVP can interfere in the crystallisation kinetics of some compounds by inhibiting the association of drug molecules to form crystal nuclei during the solvent removal from a drug-PVP solution [10,12,57,58].

In the second phase of this work, the SAS process was used to produce coprecipitates of curcumin and PVP and the effect of adjusting the solvation power of the organic solvent, pressure, temperature, initial solution concentration, mass ratio between drug and polymer and solution flow rate were explored. Five experiments were run in triplicates and the relative standard deviation of total product recovery and curcumin recovery was typically below 5%, showing that the conditions were well controlled. The results shown correspond to the mean values.

3.2.1. Effect of solvent mixture composition

Knowing that the relative composition of acetone in the solvent mixture affects the recovery of PVP particles, mixtures of acetone-ethanol with increasing acetone volume fraction from 0 to 90% were used for the coprecipitation experiments (#8-14). Tests were carried out at the same conditions used for the precipitation of the single compounds (40°C, 9.0 MPa, X_{CO2} = 0.98 and 10 mg/ml overall solution concentration) with drug/polymer mass ratio of 1:3. 100% acetone was not used because a clear solution containing both compounds could not be obtained at the specified concentration. The effect of adjusting the solution supersaturation through the manipulation of the solvent power, while keeping the overall solution concentration constant, is demonstrated in this section. Similarities in the vapour-liquid equilibria of the systems CO_2-ethanol and CO_2-acetone can be seen in the supplementary material.

The first interesting result can be seen by comparing run #1 (PVP alone), run #5 (curcumin alone) and run #8 (coprecipitation) performed at the same conditions with ethanol as solvent. For the single compounds no powder was obtained, while in the coprecipitation the total product recovery was 43.1%. Similarly, in run #3 (PVP alone) and run #6 (curcumin alone) product recovery was 2% and 23.4%, respectively, increasing to 77.6% in run #12 when the materials were coprecipitated from a 50-50 Ac-EtOH solution (**Table 1**). These results suggest a synergistic effect in improving the supersaturation of the solution when both compounds are present and how the presence of two different solutes can affect the high pressure equilibrium of the system solvent/antisolvent, leading to different results at the same process conditions. **Fig. 3**a reveals that two different morphologies, crystals (curcumin) and irregular particles (PVP), were obtained when pure ethanol was used (run #8),

indicating that coprecipitation was unsuccessful since the compounds precipitated separately. Particle size could not be measured. It was considered that this behaviour may be indicative of precipitation outside of the supercritical region caused by the solutes elevating the critical pressure of the mixture. To test this, an experiment was performed at 12.0 MPa (run #9), far beyond the critical point of the system CO_2-ethanol (8.16 MPa [51]), to ensure supercritical conditions. Curcumin crystals could still be seen, as shown in **Fig. 3**b, suggesting that the separate precipitation is related to something other than effects on the CO_2-ethanol vapour-liquid equilibrium. As the solubility in ethanol of curcumin and PVP is approximately 5 mg/ml and 315 mg/ml, respectively, the difference in the supersaturation ratio (initial concentration/solubility) of the two compounds might be so high that simultaneous precipitation would not be achieved. On the other hand, higher pressure increased product recovery from 43.1% (run #8) to 63.1% (run #9), suggesting a decrease in the solute solubility in the fluid phase.

In run #10, the addition of 10% acetone resulted in a successful coprecipitation, as shown in **Fig. 3**c. Spherical, largely uniform particles were produced and curcumin rod/filament morphology could no longer be detected indicating that curcumin is well dispersed in the polymer matrix. A possible reason for this behaviour may be that addition of acetone to ethanol simultaneously decreases the solubility of PVP and increases the solubility of curcumin (as it does at room temperature), leading to more similar supersaturation ratios of the two solutes when mixed with CO_2. The composite material retained the morphology of the polymer as previously observed in several studies with PVP-drug [33], demonstrating that the precipitation behaviour is now dominated by PVP. In **Fig. 4**a it is interesting to observe the gradual increase in the total product recovery (from 43.1 to 90.0%) and decrease in the mean particle size of coprecipitates (from 327 to 51 nm) by increasing the acetone content from 0 to 90%. SEM images shown in **Fig. 3**c,d,e,f,g clearly demonstrates this tendency. The size range changed from sub-microparticles to nanoparticles and the particle size distribution narrowed (**Fig. 4**b). De Marco et al. [24] explained that the variation of the solvent mixture composition can affect the SAS process in two different ways: by changing the solvation power of the solvent (ability of the solvent to dissolve the solute at fixed conditions) and/or the mixing behaviour of the injected solution

with CO_2 (large or sharp pressure transition range from two-phase to one-phase mixing). In terms of mixing regimes, ethanol and acetone have been shown to have similar behaviour (sharp transition pressure range) [24], therefore the decrease in the mean particle size can be explained by the decrease in the solvation power as acetone is added to the solvent mixture. Other authors have suggested that acetone repels the polymer molecules which then tend to be arranged in a more compact configuration, consequently decreasing particle size [24,53]. The amount of curcumin retained in the filter gradually decreased from 41.1 to 0.8% as the acetone content increased from 0 to 90% (**Table 1**). It is not clear why different amounts of material gets trapped in the filter walls at different operating conditions, hence further investigations will be carried out in future work. Possibly, when more acetone is present in the system, higher supersaturation can be achieved and the material precipitates in the first centimetres of the precipitator. The concentration of the fluid phase decreases and less curcumin is left to nucleate within the thimble walls when passing through it. A decrease in the degree of particle coalescence was also observed with the addition of acetone, explained by the fact that acetone experiences a higher volume expansion than alcohols when in contact with sc-CO_2 [59,60], being more efficiently removed from the precipitating particles.

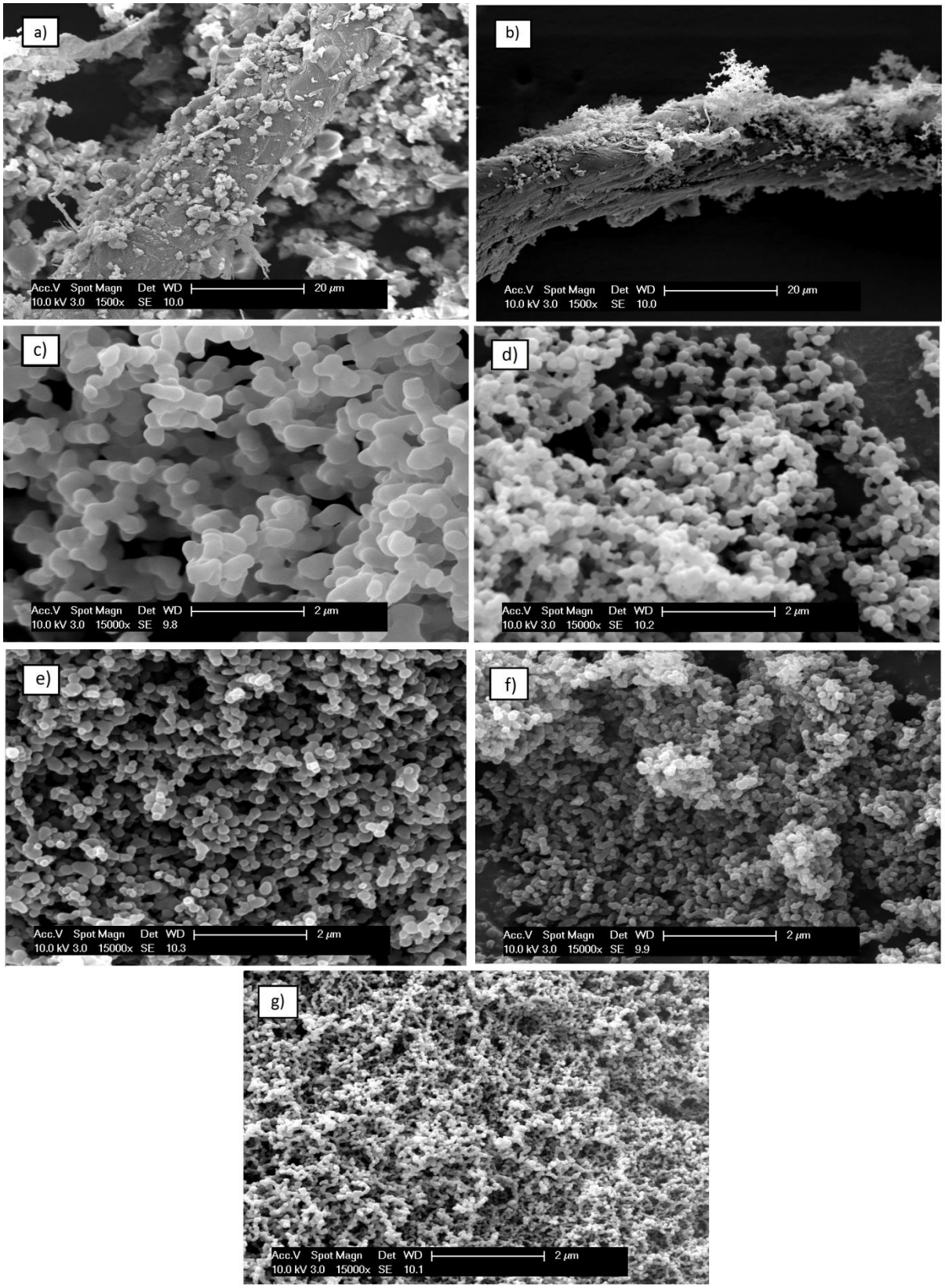

Fig. 3. SEM images of CURC/PVP processed from pure ethanol at 40°C, 1.0 ml/min, 1:3 CURC/PVP ratio and different pressures: a) 9.0 MPa (run #8); b) 12.0 MPa (run #); and samples processed at 9.0 MPa, 40°C, 1.0 ml/min, 1:3 CURC/PVP ratio from different Ac-EtOH compositions: c) 10-90 (run #10); d) 30-70 (run #11); e) 50-50 (run #12); f) 70-30 (run #13); g) 90-10 (run #14).

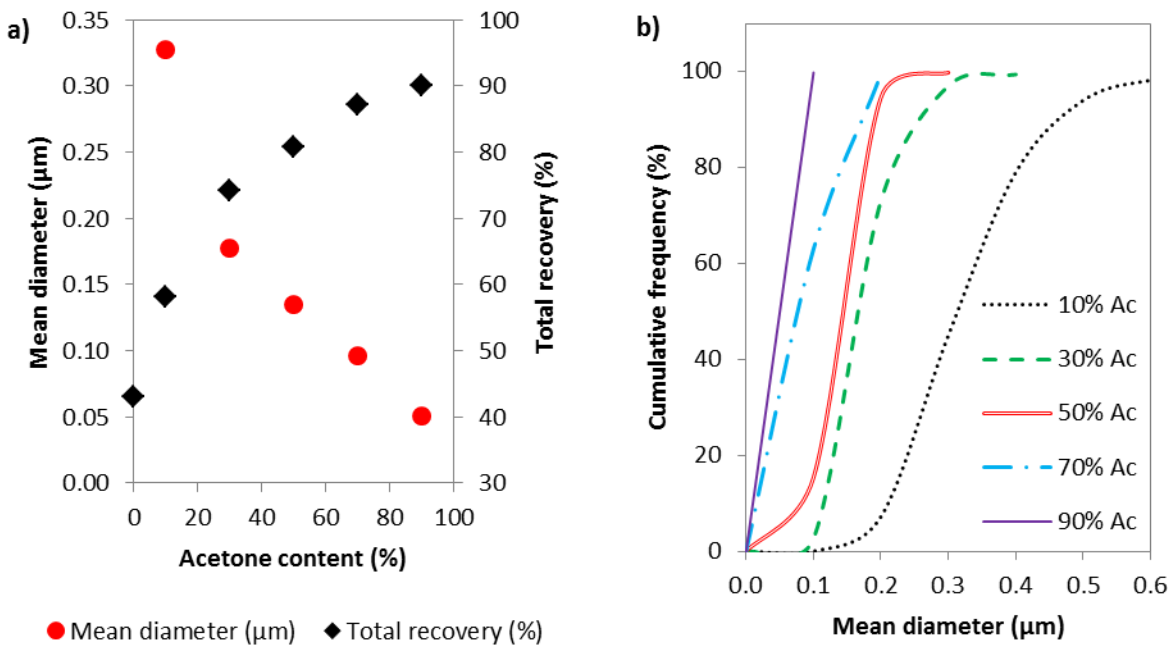

Fig. 4. Results for coprecipitates obtained from solutions with different acetone (Ac) contents at 9.0 MPa and 40°C (run #8, #10-14, **Table 1**): a) mean diameter and total product recovery; b) particle size distribution.

Fig. 5a shows the comparison between curcumin content in the processed samples and in the feed solutions. For all experiments, the contents before and after processing are similar; therefore the values of curcumin recovery are close to the respective values of the total product recovery, gradually increasing from 45.5 (run #8) to 89.2% (run #14) with increasing acetone content. This demonstrates that the conditions selected are appropriate to precipitate both compounds in the designed proportion since their proportion was kept almost the same in the feed solution and in the coprecipitated powder. It is also interesting to observe in **Fig. 5**b that no degradation of curcumin occurred after SAS processing. Curcumin retention time (highest peak) was around 7.6 minutes with impurities being detected slightly before (small peak). By comparing the area of the peaks, curcumin concentration was determined to be around 90% in all samples (raw curcumin, #6 and #13). As it is not the aim of this work, the nature of the impurities was not determined, however curcumin is known to be found with other two curcuminoids (demethoxycurcumin, and bis-demethoxycurcumin) in turmeric extracts which have been analysed in many works elsewhere [40,61–63].

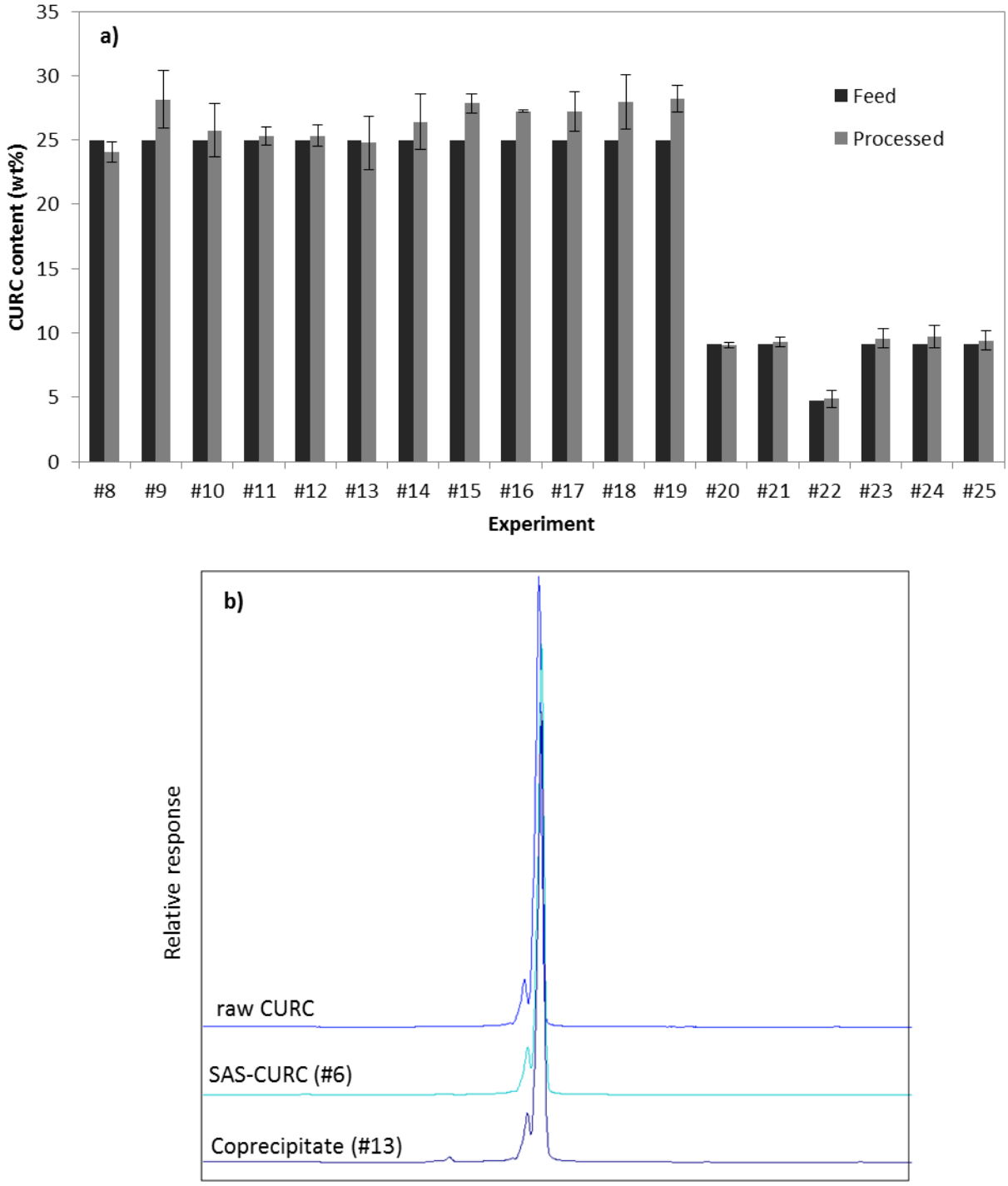

Fig. 5. a) Curcumin content as fraction of the total solute in the feed solutions and SAS-processed samples analysed by UV-visible spectrophotometer; b) HPLC measurements of raw curcumin and processed samples. Experiment conditions are shown in **Table 1**.

The effect of solvent can also be analysed in runs #21-22 (**Fig. 6**a,b) performed at 1:10 CURC/PVP ratio and runs #24-26 (**Fig. 6**d,e,f) performed at 1:10 CURC/PVP ratio and 0.5 ml/min. Similar trends as runs #10-14 were observed in terms of total product recovery, curcumin recovery (**Table 1**) and particle size (**Fig. 6**), supporting the discussion previously presented. As curcumin recovery did not increase for acetone content higher than 70% (**Table 1**), a 70-30 Ac-EtOH solution was selected in order to analyse the effect of other operational parameters on particle size and recovery. Moreover, 30% of ethanol gives flexibility to work with large amounts of PVP. Therefore, the next experiments will be compared with run #13, analysing the effect of pressure, temperature and initial solution concentration.

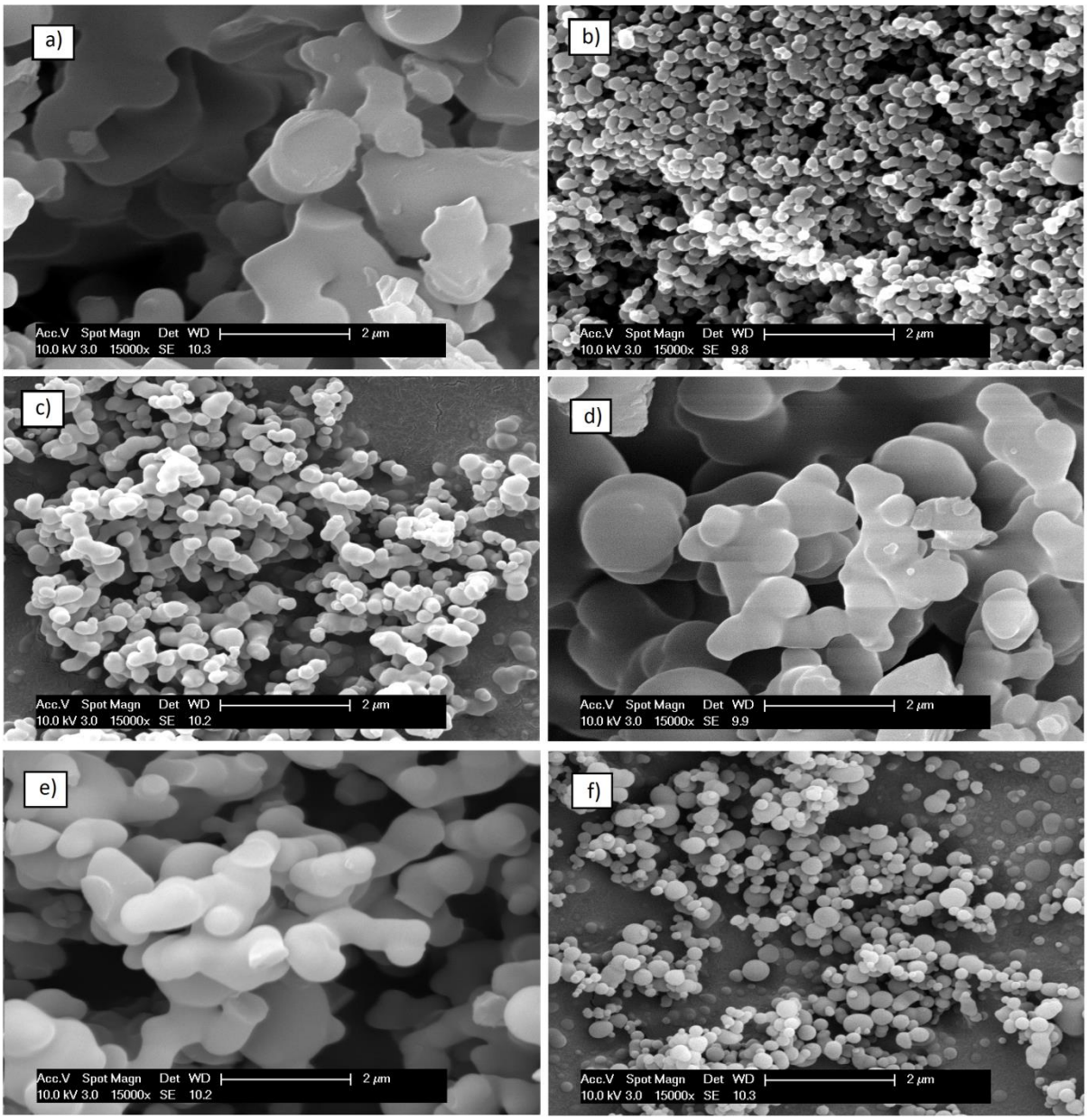

Fig. 6. SEM images of CURC/PVP processed at 40°C, 9.0 MPa, 1.0 ml/min from different Ac-EtOH compositions and CURC/PVP ratios: a) 50-50, 1:10 (run #21); b) 70-30, 1:10 (run #22); c) 70-30, 1:20 (run #23); and processed at 0.5 ml/min: d) pure EtOH, 1:10 (run #24); e) 10-90, 1:10 (run #25) f) 70-30, 1:10 (run #26).

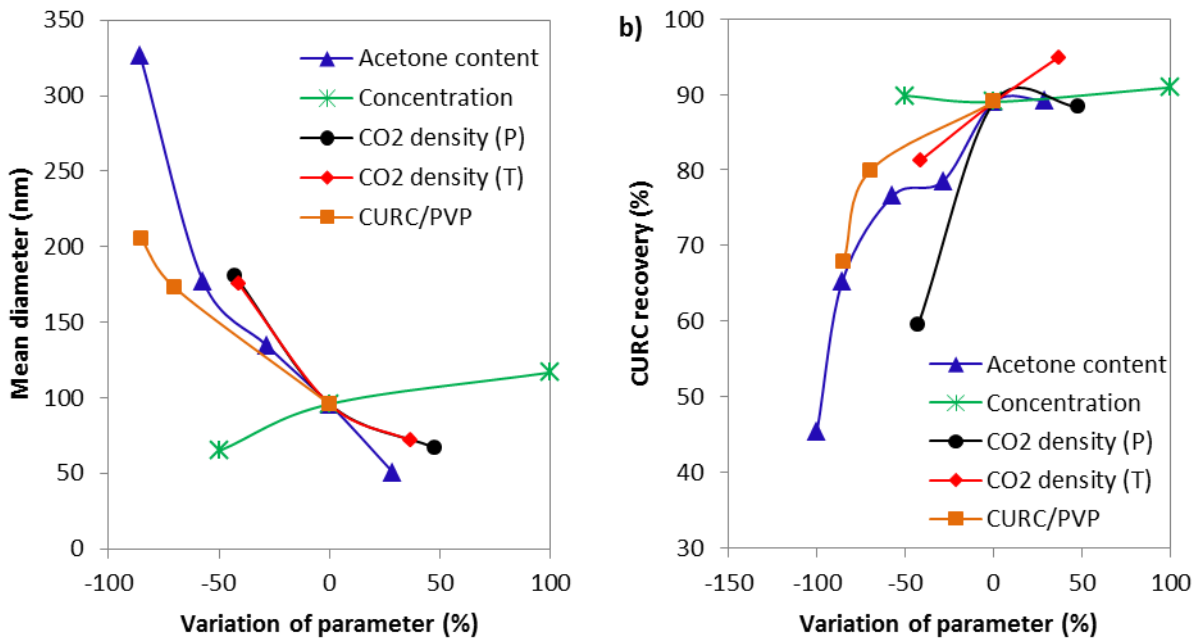

Fig. 7. Values of a) mean particle diameter and b) curcumin recovery as a function of the variation of different operational parameters in comparison with run #13 (centre point).

3.2.2. Effect of pressure

The effect of pressure was analysed by keeping the operational conditions the same as in run #13 (40°C, 1 ml/min, X_{CO2} = 0.98, 1:3 CURC/PVP ratio and 10 mg/ml overall solution concentration in a 70-30 Ac-EtOH solution) and changing the pressure from 9.0 MPa to 8.0 MPa (#15) and 12.0 MPa (#16).

As the critical pressures of the CO_2-ethanol and CO_2-acetone systems are approximately 8 MPa at 40°C, the operational point in run #15 might be located in the biphasic region. The density of CO_2 under these conditions (277.9 kg/m^3 [64]) is around 43% lower than at 9.0 MPa (485.5 kg/m^3 [64]). This lowers the power of CO_2 to solubilise the organic solvents and leads to a less effective supersaturation, which might explain the large increase in particle size from 96 nm (#13) to 181 nm (run #15, **Fig. 8**a) and decrease in curcumin recovery from 89.0 (#13) to 59.6% (#15). A high

proportion (around 21%) of the curcumin injected was retained in the cellulose thimble probably due to the presence of liquid in the precipitator (operating point in the biphasic region). When the pressure was increased to 12.0 MPa (#16, **Fig. 8**b), the CO_2 density increased by 48% and the opposite effect was observed for particle size which decreased to 67 nm. While product recovery (curcumin + PVP, 79.1%) was lower than at 9.0 MPa, curcumin recovery was not much affected, indicating that at higher pressure the precipitation of PVP is less favourable. **Fig. 7** illustrates how the mean particle diameter of coprecipitates and curcumin recovery varies from the central experiment (#13) as a function of the variation in the CO_2 density with pressure and other operational parameters, which will be discussed in the following sections.

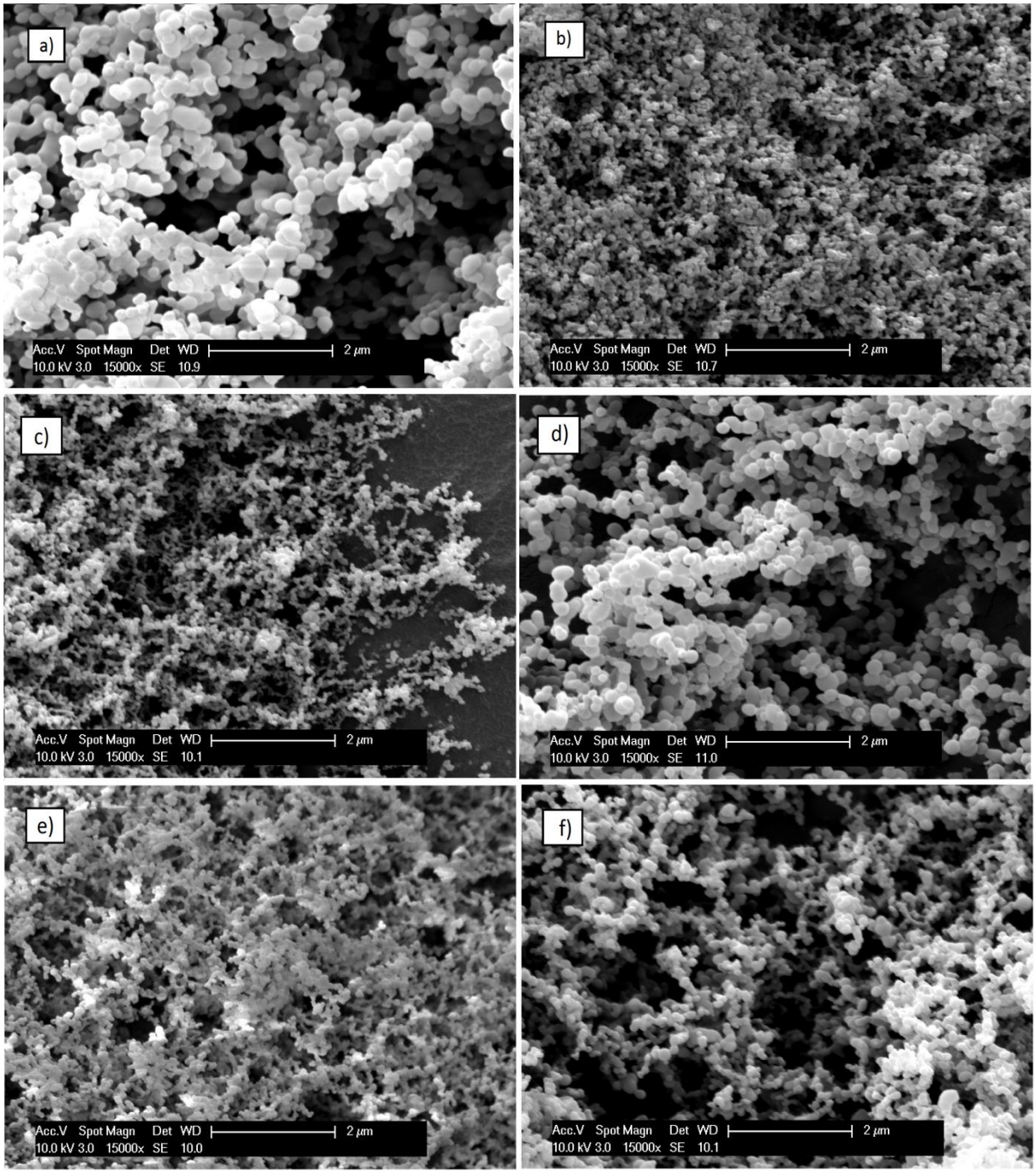

Fig. 8. SEM images of CURC/PVP processed at different conditions: a) run #15 (8.0 MPa); b) run #16 (12.0 MPa); c) run #17 (35°C); d) run #18 (50°C); e) run #19 (5 mg/ml); f) run #20 (20 mg/ml). The complete set of operational conditions is shown in **Table 1**.

3.2.3. Effect of temperature

The effect of temperature was analysed by keeping the operational conditions the same as in run #13, (9.0 MPa, 1 ml/min, X_{CO2} = 0.98, 1:3 CURC/PVP ratio and 10 mg/ml overall solution concentration

in a 70-30 Ac-EtOH solution) which was performed at 40°C, and changing the temperature to 35°C (#17) and 50°C (#18).

Fig. 8c,d shows the particles obtained at 35°C (#17) and 50°C (#18) measuring 72 and 176 nm, respectively. At 35°C the density of CO_2 is 662.1 kg/m^3 (36% higher than 485.5 kg/m^3 at 40°C[64]) while at 50°C it is equal to 285.0 kg/m^3 (41% lower than at 40°C). It is interesting to observe in **Fig. 7**a that similar CO_2 density variations from the central experiment (run #13) caused by temperature and pressure lead to the production of coprecipitates with similar particle sizes. Experiments performed at high CO_2 density (low temperature or high pressure) yielded smaller particles due to the improved solvation power of CO_2, while the opposite happened with a decrease in CO_2 density (high temperature or low pressure). These results demonstrate the relevance of the fluid density in designing SAS experiments but it is also important to be aware that other parameters such as fluid viscosity and solute vapour pressure might play a role in determining particle size as the temperature is changed.

Although similar particle sizes were obtained in runs #15 and #18 (low density) and runs #16 and #17 (high density), both changes in pressure had a negative effect on curcumin recovery (**Fig. 7**b). In contrast, at 35°C almost all curcumin was recovered, possibly because the vapour pressure and solubility of curcumin in the fluid phase decreased.

3.2.4. Effect of solution concentration

The effect of concentration was analysed by keeping the operational conditions the same as in run #13 (9.0 MPa, 40°C, 1 ml/min, X_{CO2} = 0.98, 1:3 CURC/PVP ratio and 70-30 Ac-EtOH solution) and changing the overall concentration from 10 mg/ml (run #13) to 5 mg/ml (run #19) and 20 mg/ml (run #20). The same amount of material was delivered to the precipitator but the solution volume was adjusted (doubled or halved) to obtain the desired concentration.

A low impact on precipitation was observed. In fact, curcumin recovery changed less than 2% as the concentration was increased or decreased (**Fig. 7**b). Particle size decreased to 65 nm at lower concentration (**Fig. 8**e) and increased to 117 nm at higher concentration (**Fig. 8**f), also demonstrating a small influence of concentration (**Fig. 7**a). Although higher supersaturation occurs in more

concentrated solutions, particle growth by condensation is also intensified [50], explaining the results obtained here.

3.2.5. Effect of drug/polymer mass ratio

The effect of CURC/PVP mass ratio was studied by decreasing the ratio from 1:3 (run #13) to 1:10 (run #22) and 1:20 (run #23). All other operating conditions were kept the same as run #13 (9.0 MPa, 40°C, 1 ml/min, X_{CO2} = 0.98, 10 mg/ml overall solution concentration in a 70-30 Ac-EtOH solution). In order to keep the overall concentration constant, the decrease in CURC/PVP ratio was achieved by simultaneously decreasing the concentration of curcumin and increasing the concentration of PVP.

The morphologies of the particles produced at 1:3, 1:10 and 1:20 CURC/PVP ratios are shown in **Fig. 3**f and **Fig. 6**b,c, respectively. The results in **Table 1** demonstrate a gradual decrease in total product recovery from 87.1% to 79.7% and 69.2% as CURC/PVP ratio decreased. Similarly, curcumin recovery decreased (**Fig. 7**b) since the curcumin content in the processed sample and feed solution were almost unchanged (**Fig. 5**a) (the ratio between the drug and polymer remained the same in the precipitated powder). On the other hand, particle size increased from 96 nm to 173 nm and further to 205 nm in these experiments (**Fig. 7**a). This behaviour has been reported before for the coprecipitation of PVP with other APIs [8,9]. Although the overall concentration was kept constant, the increase in the concentration of the polymer (from 7.5 mg/ml at 1:3 ratio to 9.5 mg/ml at 1:20 ratio) might have increased the viscosity of the solution, which decreases the nucleation rate and lead to the formation of larger and more coalescing particles [48,65,66]. It is also important to highlight that an increase in the concentration of PVP can additionally affect the particle-fluid interfacial tension. This parameter might significantly influence particle size, as demonstrated by Erriguible et al. [67].

Runs #12 (**Fig. 3**e) and #21 (**Fig. 6**a) performed with 50% Ac-EtOH solution can also be used to analyse the effect of decreasing the drug/polymer ratio from 1:3 to 1:10. Once again, the same trend was observed: a decrease in total product recovery and curcumin recovery and increase in particle size. It was also noticed that at higher PVP concentration more acetone is needed in the solvent mixture to generate non-coalescing particles. For coprecipitates with 1:3 CURC/PVP ratio, particles become discrete with 30% acetone (**Fig. 3**d). However, highly coalescing material is still obtained at

1:10 ratio (**Fig. 6**a) when the acetone content was 50% (run #21), which prevented the measurement of the particle size. The reason for this behaviour might be that by increasing PVP concentration in the solution, the viscosity of the liquid phase increases, decreasing the supersaturation and nucleation rate and leading to a less efficient mixing and solvent removal from the particles, as previously explained. Therefore, the addition of acetone, which is less viscous and poorer solvent to PVP than ethanol, favours the formation of discrete particles.

3.2.6. Effect of solution flow rate

The effect of solution flow rate was analysed by keeping the operational conditions unchanged (40°C, 9.0 MPa and 10 mg/ml overall solute concentration) and decreasing the solution flow rate to 0.5 ml/min (X_{CO2} = 0.99) for a 70-30 Ac-EtOH solution and 1:10 CURC/PVP ratio. This CURC/PVP ratio was selected because the effect of particle coalescence was more pronounce at 1:10 than at 1:3 and therefore we wanted to investigate the possibility of producing discrete particles with higher PVP content. Run #26 (0.5 ml/min) can be compared to run #22 (1.0 ml/min) as all other operating conditions were not changed. The SEM image presented in **Fig. 6**f (run #26) shows the formation of discrete sub-microparticles compared to the less discrete particles of run #22 (**Fig. 6**b).

Solution flow rate is supposed to have a minor impact on particle size [50,68,67] since it may cause two opposite effects in relation to the supersaturation. For instance, a decrease in the solution flow rate can lead to a less efficient mixing (which decreases the local supersaturation) and it can also decrease the solvent composition in the fluid phase which decreases the solute solubility and hence increases the maximum attainable supersaturation. Therefore, lower impact is expected comparing to other parameters which affect the vapour-liquid phase equilibrium (pressure and temperature) [50]. As particle size, morphology and product recovery are affected in different extent by these phenomena, it was observed a small increase in particle size from 173 nm (run #22) to 220 nm (run #26), while product recovery was not significantly affected, with values close to 80% (**Table 1**). Particle coalesce was reduced at lower flow rates possibly due to the fact that there is more time for the precipitating particles to dry before they collide with each other, as explained by Gokhale et al. [53]. Similar effects

of the solution flow rate on particle size have been reported elsewhere for the precipitation of PVP alone by SAS [53].

3.3. X-Ray Diffraction (XRD)

The degree of crystallinity of the samples was analysed by XRD. **Fig. 9** shows that curcumin alone processed by SAS (SAS-CURC, run #7) is less crystalline than raw curcumin (CURC) as the intensity of the peaks decreased. The physical mixture (PM 1:3) kept all the curcumin characteristic peaks but with lower heights than raw CURC due to the presence of PVP, which is an amorphous polymer. The comparison of the PM (1:3) with the coprecipitates shows that amorphous formulations were formed in all coprecipitates (runs #11, #13, #14).

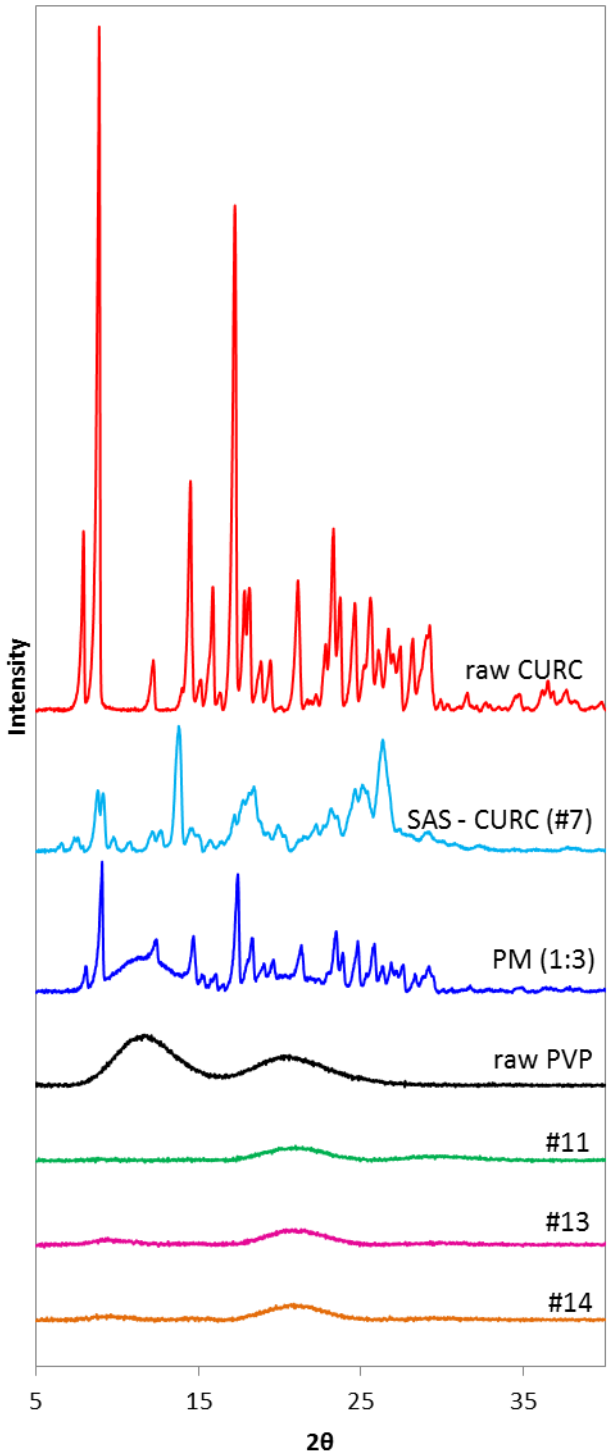

Fig. 9. XRD patterns of raw materials and processed samples. Experiment conditions are shown in **Table 1**.

3.4. Differential Scanning Calorimetry (DSC)

Differential Scanning Calorimetry (DSC) was used to access the degree of crystallinity of the samples and possible interactions between curcumin and PVP after processing. **Fig. 10** shows a sharp

endothermic peak corresponding to the melting point of raw curcumin at T_m = 182°C and enthalpy of fusion of ΔH_f = 130.9 J/g, indicating the crystallinity of the compound. Other works have reported similar values for the melting point of unprocessed curcumin but fusion enthalpy varying from 93 – 121 J/g [14,16,56,69,70], which can be explained by differences in the purity of the sample, not always specified, and differences in the crystal form. PVP, on the other hand, does not show any melting point peak, demonstrating its amorphous structure and glass transition at T_g = 150°C (midpoint of the change in heat capacity). In the physical mixture (PM 1:3) the curcumin characteristic peak was slightly shifted to lower temperature. This behaviour has been observed by other researchers and may be attributable to a solvent effect of PVP [14,16]. For the SAS coprecipitate obtained in run #13, no endothermic peak could be detected in the region of curcumin melting point which indicates that amorphous curcumin was obtained after SAS processing with PVP, confirming the XRD results (section 3.3). The presence of a single T_g supports the hypothesis of a single phase and the decrease in T_g compared to the one of PVP is attributed to the plasticizing effect of the drug molecularly dispersed in the polymeric matrix [13,71].

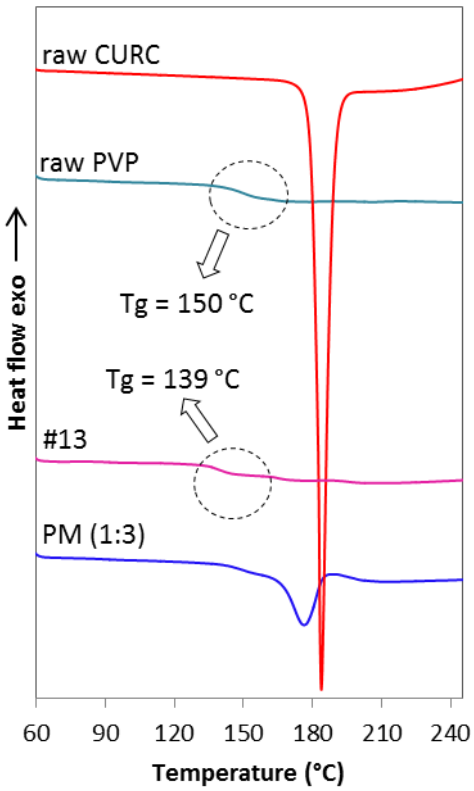

Fig. 10. DSC thermograms of raw materials and coprecipitate (#13). Experiment conditions are shown in **Table 1**.

3.5. Fourier Transform Infrared Spectroscopy (FTIR)

The infrared spectra of the compounds before and after processing were analysed in order to identify possible interactions between curcumin and PVP. **Fig. 11** shows the results obtained. Raw curcumin (CURC) presents an absorption band at 3504 cm^{-1} corresponding to O-H stretching vibration. Other peaks can be identified at 1626 cm^{-1} (C=O, C=C), 1601 cm^{-1} (C=C aromatic), 1427 cm^{-1} (C-O phenol), 1025 cm^{-1} (C-O-C), 960 cm^{-1} (benzoate trans-CH) and 855 cm^{-1} (C-H aromatic) [39,72]. The FTIR spectrum of PVP shows a peak at 3466 cm^{-1} assigned to the stretching vibration of O-H and other peaks at 2883, 1651 and 1284 cm^{-1}, corresponding to C-H, C=O and C-N, respectively [10,39].

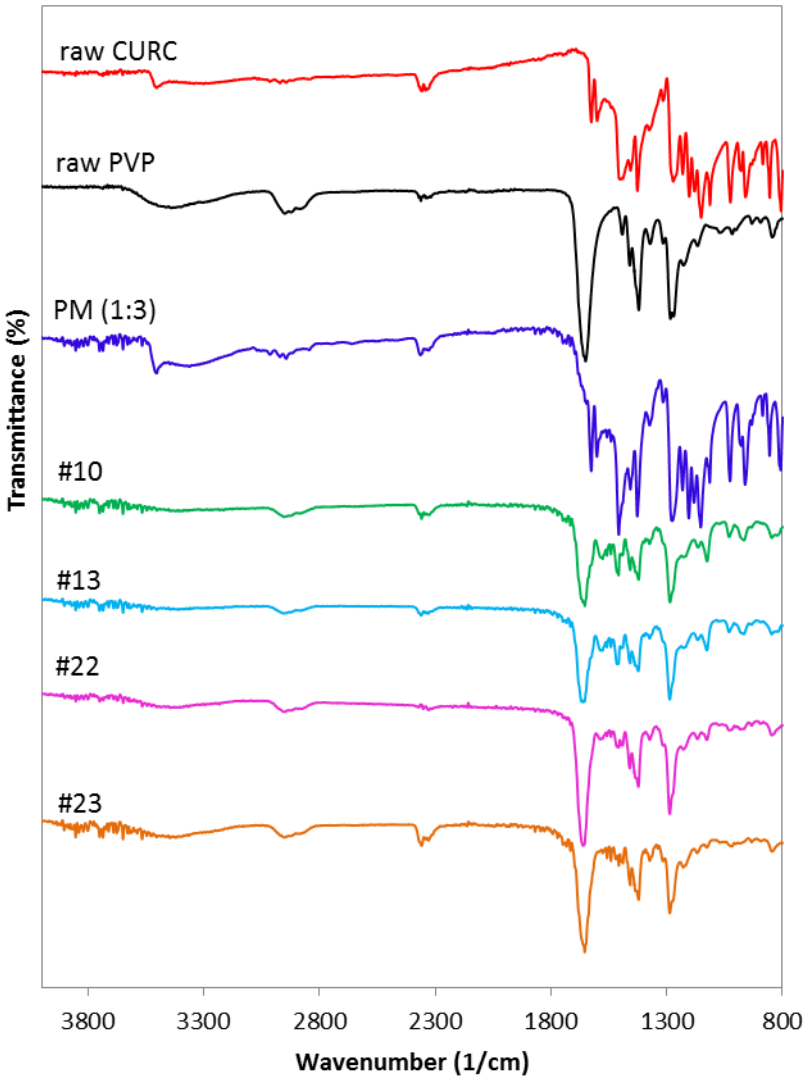

Fig. 11. IR spectra of raw materials and processed samples. Experiment conditions are shown in **Table 1**.

The spectrum of the physical mixture (PM 1:3) is similar to the addition of the individual spectra of curcumin and PVP, which indicates that no interaction between them has occurred. On the other hand, for the samples of CURC/PVP processed by SAS (#10, #13, #22, #23), the O-H characteristic peak (3504 cm^{-1}) from curcumin has disappeared. This can be ascribed to an intermolecular interaction, such as hydrogen bonding, between the O-H of curcumin and the C=O of PVP [16]. This behaviour is compatible with the observations of other researchers [16,39,73,74] and might explain the change in the structure of curcumin from crystalline to amorphous (sections 3.3 and 3.4) and the improvement in the aqueous apparent solubility (section 3.6) and dissolution properties of curcumin formulations (section 3.7).

3.6. Drug apparent solubility

The apparent solubility of raw curcumin (CURC), SAS-processed curcumin (SAS-CURC, #7), CURC/PVP physical mixtures (PM) and SAS coprecipitates was determined in water at 25°C. Unprocessed curcumin has not shown any absorbance at these conditions, while other authors have measured 0.006 µg/ml after dissolution for 12h in water [39] and 0.5 µg/ml after dissolved in saline solution and centrifuged at 12,000 rpm for 10 min (25 °C) [36]. The different conditions and method used explain the different results obtained. The low water solubility of curcumin is one of the main causes of its low bioavailability [3].

The apparent solubility of curcumin processed by SAS alone was equal to 0.06 µg/ml, which is still very low. The addition of PVP was found to improve curcumin apparent solubility in the physical mixtures. 0.3 µg/ml was measured in the mixture at 1:3 CURC/PVP, while 4.4 µg/ml was obtained at 1:10 ratio. This might be explained by a possible decrease in the surface tension of water in the presence of PVP, which enhances the wetting of the curcumin crystal surface [11,65].

CURC/PVP coprecipitates were produced in an attempt to further increase curcumin apparent solubility. The apparent solubility of raw CURC, physical mixtures and curcumin formulations are presented in **Fig. 12**a. In runs #11 and #13 the apparent solubility increased around 100 times

compared with the physical mixture (1:3), while in run #14 an increase of more than 600 times was obtained. By decreasing CURC/PVP ratio, this effect was even more remarkable (**Fig. 12**a**)**. In runs #22 and #26 the measured values were 369 µg/ml and 474 µg/ml, respectively. Other authors have also reported an improvement in drug apparent solubility as PVP content increases [74]. This was attributed to the formation of a water-soluble complex between drug and PVP, which was confirmed by FTIR test (section 3.5). Chhouk et al. [39] reported a curcumin apparent solubility of 2.34 µg/ml in a formulation with PVP while Kurniawansyah et al. [37] obtained the highest value equal to 77.6 µg/ml for a ternary system containing curcumin, PVP and methyl-β-cyclodextrin in a ratio of 1:4:4 at pH 4.5.

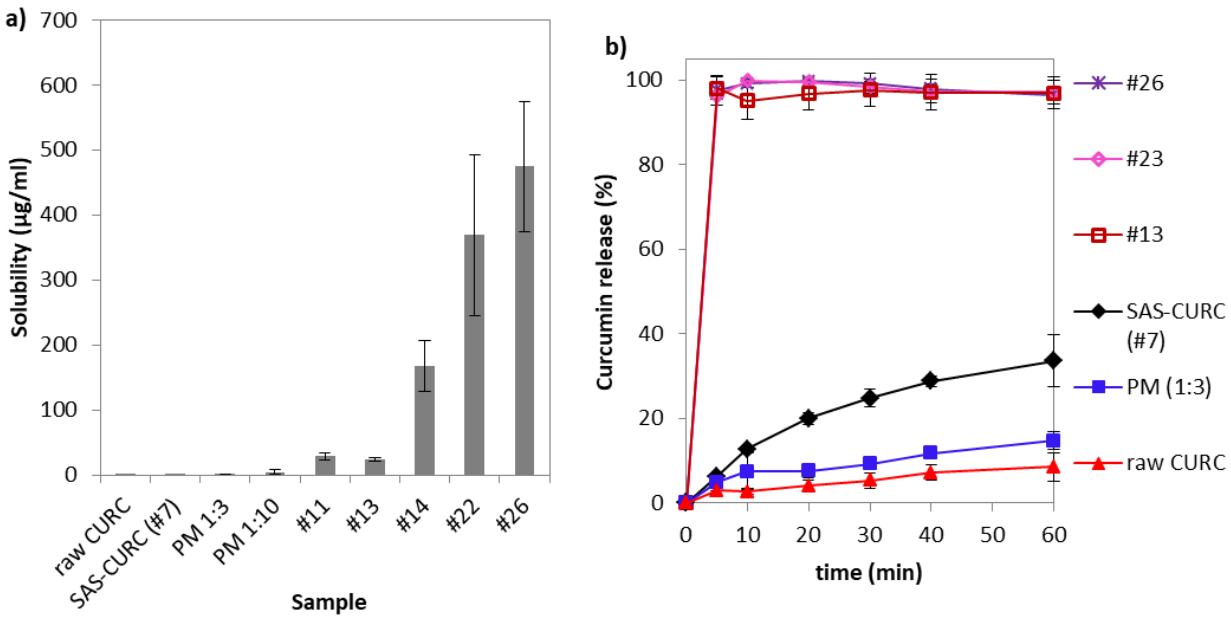

Fig. 12. a) Apparent solubility and b) dissolution profile of raw curcumin (CURC), physical mixtures (PM) and processed samples. Experiment conditions are shown in **Table 1**.

3.7. In vitro dissolution studies

The dissolution profile of coprecipitates (#13, #23, #26), raw curcumin (CURC), physical mixture (PM 1:3) and curcumin processed by SAS alone (SAS-CURC, #7) was investigated in water + 0.25% w/v SDS. The surfactant SDS was added to allow for a shorter dissolution study and minimise the impact of curcumin degradation in the results. Moreover, when no SDS was used, there was no discrimination among the release profiles of the raw CURC, PM (1:3) and SAS-CURC (#7) due to

their absorbance values being too close to the minimum detection limit of the UV-visible spectrophotometer used (results not shown).

Fig. 12b shows the dissolution profiles for the various samples in water + 0.25% w/v SDS. PM (1:3) releases faster than raw CURC, which is due to the improvement in curcumin wetting and solubility in the presence of PVP, as discussed in section 3.6. The release of SAS-CURC (#7) is faster than the physical mixture (1:3), despite having lower apparent solubility in water (section 3.6), as a result of the smaller size of the curcumin crystals (**Fig. 2**c,d). All the coprecipitates analysed dissolved significantly faster than raw CURC and PM (1:3), with complete release being obtained in the first 10 minutes. In the same period of time, raw CURC, PM (1:3) and SAS-CURC (#7) released only 3.2%, 7.5% and 12.8% of curcumin, respectively. These results, in conjunction with the observations of particle morphology, thermal behaviour and measurements of curcumin recovery, demonstrate that coprecipitates with high curcumin content and improved dissolution properties were successfully produced by SAS. The enhancement in the curcumin dissolution profile can be attributed to the formation of smaller particles with increased apparent solubility (section 3.6) and reduced crystallinity compared to raw CURC (section 3.3).

Two mechanisms are suggested to for the precipitation of composite materials: homogeneous nucleation, which produces a solid mixture in which each particle if formed by only one component; and heterogeneous nucleation, which generates particles composed of both materials (coprecipitates) [33]. By the results presented in this work, it is believed that heterogeneous nucleation happened, leading to the formation of composite particles. In any case, the aim of the work was successfully achieved, as the dissolution properties of curcumin were significantly improved.

4. Conclusions

In this work, the coprecipitation of curcumin and PVP by SAS was successfully achieved from different solvent mixtures of acetone and ethanol. The results showed that the composition of the solvent mixture plays a major role in determining particle size, particle size distribution and curcumin recovery. Particle size varied from sub-microparticles (327 – 135 nm) to nanoparticles (96 - 51 nm) and the curcumin recovery increased from 45.5 to 89.2% as the relative composition of acetone in the

ethanol-acetone mixture was increased. The highest curcumin recovery (95%) was obtained at low temperature (35°C) for a 70-30 Ac-EtOH solution. It was also observed an improvement in curcumin apparent solubility of around 600 times compared with the physical mixture and, consequently, a much faster release. These results are explained by the solid state analyses which have demonstrated the formation of amorphous curcumin-PVP coprecipitates.

Competing interests

The authors would like to declare that there are no competing interests.

Acknowledgements

The authors would like to acknowledge the financial support from National Council for Scientific and Technological Development (CNPQ, Brazil) through Science Without Borders Program and Gabor Dravavolgyi for his help in the HPLC.

Vitae

Ravenna Lessa Matos

Ravenna is PhD student at the University of Birmingham. Her research project focuses on the use of supercritical fluids to solve two major challenges in the development of pharmaceutical powder formulations: flowability and dissolution.

Tiejun Lu

Dr Lu is professional, PhD qualified, with over thirty years research experience in solvent extraction particularly in the application of supercritical fluids. Worked on process design and product

development for commercial and research council sponsored projects that have included the application of reactions, separation and processing of natural products, oils, fine chemicals in supercritical and conventional fluid media.

Valentina Prosapio

Dr Valentina Prosapio awarded her Ph.D. in Chemical Engineering in Italy at the University of Salerno in 2016. Her doctoral project was about the "Micronization by supercritical antisolvent precipitation processes", in which she investigated the influence of the solvent on particle morphology, the processing of water-soluble compounds and the polymer/drug coprecipitation. Thereafter, she moved to the UK and started to work as a Research Fellow at the University of Birmingham. Her current research focuses on the development/optimisation of drying techniques and the encapsulation/incorporation of active compounds into polymeric carriers for controlled drug delivery.

Christopher McConville

Dr McConville is senior lecturer is pharmaceutics at the University of Birmingham School of Pharmacy with expertise in drug delivery, formulation, dosage form design, pharmaceutical analysis and GMP manufacturing. He specialises in solubility enhancement, oral drug delivery, implantable devices and nanoparticles. He has also spent time in the pharmaceutical industry and has a great understanding of the regulatory requirements. He has taken a number of formulations from research and development to Phase III clinical testing. He has collaborations with clinical, regulatory and industrial partners to ensure the swift translation of any product from the lab to the clinic.

Gary Leeke

Professor Leeke is Chair in Chemical Engineering and Head of the Bioenergy and Resource Management Centre. His research is largely focused on recycling enabling technologies, energy production and energy reduction through the design and development of robust resilient processes that lead to new and improved products. He has over 20 years' experience in supercritical fluid technology from fundamentals to large scale developments.

Andrew Ingram

Dr Andy Ingram lectures in multiphase processes, focussing on particle/fluid systems. Research interests focus on particle technology with application to pharmaceutical, food, minerals and catalyst industries, amongst others.

References

[1] S.C. Gupta, S. Patchva, B.B. Aggarwal, Therapeutic Roles of Curcumin: Lessons Learned from Clinical Trials, Am. Assoc. Pharm. Sci. J. 15 (2013) 195–218. doi:10.1208/s12248-012-9432-8.

[2] O. Naksuriya, S. Okonogi, R.M. Schiffelers, W.E. Hennink, Curcumin nanoformulations: A review of pharmaceutical properties and preclinical studies and clinical data related to cancer treatment, Biomaterials. 35 (2014) 3365–3383. doi:10.1016/j.biomaterials.2013.12.090.

[3] R.I. Mahran, M.M. Hagras, D. Sun, D.E. Brenner, Bringing Curcumin to the Clinic in Cancer Prevention: a Review of Strategies to Enhance Bioavailability and Efficacy, AAPS J. 19 (2017) 54–81. doi:10.1208/s12248-016-0003-2.

[4] L.P. Cunico, M.C. Acosta, C. Turner, Experimental measurements and modeling of curcumin solubility in CO2-expanded ethanol, J. Supercrit. Fluids. (2017) 1–8. doi:10.1016/j.supflu.2017.06.018.

[5] Z. Hussain, H. Ei, M. Wahab, F. Hussain, T.A. Ahmed, S. Khan, Exploring recent developments to improve antioxidant , anti-inflammatory and antimicrobial efficacy of curcumin : A review of new trends and future perspectives, Mater. Sci. Eng. C. 77 (2017) 1316–1326. doi:10.1016/j.msec.2017.03.226.

[6] A. Sao Pedro, S.D. Villa, P. Caliceti, S.A.B.V. De Melo, E.C. Albuquerque, A. Bertucco, S. Salmaso, Curcumin-loaded solid lipid particles by PGSS technology, J. Supercrit. Fluids. 107 (2016) 534–541. doi:10.1016/j.supflu.2015.07.010.

[7] Z. Hussain, H.E. Thu, S. Ng, S. Khan, H. Katas, Nanoencapsulation , an efficient and promising approach to maximize wound healing efficacy of curcumin : A review of new trends and state-of-the-art, Colloids Surfaces B Biointerfaces. 150 (2017) 223–241. doi:10.1016/j.colsurfb.2016.11.036.

[8] V. Prosapio, E. Reverchon, I. De Marco, Incorporation of liposoluble vitamins within PVP microparticles using supercritical antisolvent precipitation, J. CO2 Util. 19 (2017) 230–237. doi:10.1016/j.jcou.2017.04.004.

[9] V. Prosapio, I. De Marco, M. Scognamiglio, E. Reverchon, Folic acid-PVP nanostructured composite microparticles by supercritical antisolvent precipitation, Chem. Eng. J. 277 (2015) 286–294. doi:10.1016/j.cej.2015.04.149.

[10] V. Prosapio, I. De Marco, E. Reverchon, PVP/corticosteroid microspheres produced by supercritical antisolvent coprecipitation, Chem. Eng. J. 292 (2016) 264–275. doi:10.1016/j.cej.2016.02.041.

[11] H. Sekikawa, M. Nakano, T. Arita, Dissolution Mechanisms of Drug-Polyvinylpyrrolidone Coprecipitates in Aqueous Solution, Chem. Pharm. Bull. 27 (1979) 1223–1230.

[12] S. Jain, N. Patel, S. Lin, Solubility and dissolution enhancement strategies: current understanding and recent trends*, Drug Dev. Indusrial Pharm. 41 (2015) 875–887. doi:10.3109/03639045.2014.971027.

[13] P. Gupta, V.K. Kakumanu, A.K. Bansal, Stability and Solubility of Celecoxib – PVP Amorphous Dispersions : A Molecular Perspective, 21 (2004) 1762–1769.

[14] A. Paradkar, A.A. Ambike, B.K. Jadhav, K.R. Mahadik, Characterization of curcumin-PVP solid dispersion obtained by spray drying, Int. J. Pharm. 271 (2004) 281–286. doi:10.1016/j.ijpharm.2003.11.014.

[15] D. Xu, S. Wang, J. Jin, X. Mei, S. Xu, Dissolution and absorption researches of curcumin in solid dispersions with the polymers PVP, Asian J. Pharmacodyn. Pharmacokinet. 6 (2006) 343–349.

[16] N. Kaewnopparat, S. Kaewnopparat, A. Jangwang, D. Maneenaun, T. Chuchome, P. Panichayupakaranant, Increased solubility, dissolution and physicochemical studies of curcumin-polyvinylpyrrolidone K-30 solid dispersions, Int. J. Medical, Heal. Biomed. Bioeng. Pharm. Eng. 3 (2009) 137–142. http://citeseerx.ist.psu.edu/viewdoc/download?doi=10.1.1.192.9888&rep=rep1&type=pdf.

[17] M.K. Modasiya, V.M. Patel, Studies on solubility of curcumin, Int. J. Pharm. Life Sci. 3 (2012) 2713–2716. doi:10.2330/joralbiosci1965.30.54.

[18] A.S. Silva, M.T. Tavares, A. Aguiar-Ricardo, Sustainable strategies for nano-in-micro particle engineering for pulmonary delivery, J. Nanoparticle Res. 16 (2014) 1–17. doi:10.1007/s11051-014-2602-0.

[19] J.S. Kim, M.S. Kim, H.J. Park, S.J. Jin, S. Lee, S.J. Hwang, Physicochemical properties and oral bioavailability of amorphous atorvastatin hemi-calcium using spray-drying and SAS process, Int. J. Pharm. 359 (2008) 211–219. doi:10.1016/j.ijpharm.2008.04.006.

[20] Y. Li, D.J. Yang, S.L. Chen, S.B. Chen, A.S.C. Chan, Comparative physicochemical characterization of phospholipids complex of puerarin formulated by conventional and supercritical methods, Pharm. Res. 25 (2008) 563–577. doi:10.1007/s11095-007-9418-x.

[21] S.F. Chow, K.Y. Wan, K.K. Cheng, K.W. Wong, C.C. Sun, L. Baum, A.H.L. Chow, Development of highly stabilized curcumin nanoparticles by flash nanoprecipitation and lyophilization, Eur. J. Pharm. Biopharm. 94 (2015) 436–449. doi:10.1016/j.ejpb.2015.06.022.

[22] P. Valeh-e-Sheyda, M. Rahimi, H. Adibi, Z. Razmjou, H. Ghasempour, An insight on reducing the particle size of poorly-water soluble curcumin via LASP in microchannels, Chem. Eng. Process. Process Intensif. 91 (2015) 78–88. doi:10.1016/j.cep.2015.03.018.

[23] F. Sadeghi, M. Ashofteh, A. Homayouni, M. Abbaspour, A. Nokhodchi, H.A. Garekani, Antisolvent precipitation technique: A very promising approach to crystallize curcumin in presence of polyvinyl pyrrolidon for solubility and dissolution enhancement, Colloids Surfaces B Biointerfaces. 147 (2016) 258–264. doi:10.1016/j.colsurfb.2016.08.004.

[24] I. De Marco, M. Rossmann, V. Prosapio, E. Reverchon, A. Braeuer, Control of particle size, at micrometric and nanometric range, using supercritical antisolvent precipitation from solvent mixtures: Application to PVP, Chem. Eng. J. 273 (2015) 344–352. doi:10.1016/j.cej.2015.03.100.

[25] R.L. Matos, T. Lu, C. McConville, G. Leeke, A. Ingram, Analysis of curcumin precipitation and coating on lactose by the integrated supercritical antisolvent-fluidized bed process, J. Supercrit. Fluids. In press. (n.d.). doi:10.1016/j.supflu.2017.12.013.

[26] E. Reverchon, I. De Marco, Mechanisms controlling supercritical antisolvent precipitate morphology, Chem. Eng. J. 169 (2011) 358–370. doi:10.1016/j.cej.2011.02.064.

[27] E. Badens, Y. Masmoudi, A. Mouahid, C. Crampon, Current situation and perspectives in drug formulation by using supercritical fluid technology, J. Supercrit. Fluids. 134 (2018) 274–283. doi:10.1016/j.supflu.2017.12.038.

[28] E. Reverchon, I. De Marco, R. Adami, G. Caputo, Expanded micro-particles by supercritical antisolvent precipitation: Interpretation of results, J. Supercrit. Fluids. 44 (2008) 98–108. doi:10.1016/j.supflu.2007.08.008.

[29] E. Reverchon, R. Adami, G. Caputo, I. De Marco, Spherical microparticles production by supercritical antisolvent precipitation: Interpretation of results, J. Supercrit. Fluids. 47 (2008) 70–84. doi:10.1016/j.supflu.2008.06.002.

[30] E. Reverchon, I. De Marco, E. Torino, Nanoparticles production by supercritical antisolvent precipitation: A general interpretation, J. Supercrit. Fluids. 43 (2007) 126–138. doi:10.1016/j.supflu.2007.04.013.

[31] I.N. Uzun, O. Sipahigil, S. Dinçer, Coprecipitation of Cefuroxime Axetil-PVP composite

microparticles by batch supercritical antisolvent process, J. Supercrit. Fluids. 55 (2011) 1059–1069. doi:10.1016/j.supflu.2010.09.035.

[32] A.Z. Chen, X.M. Pu, Y.Q. Kang, L. Liao, Y.D. Yao, G.F. Yin, Preparation of 5-fluorouracil-poly(L-lactide) microparticles using solution-enhanced dispersion by supercritical CO2, Macromol. Rapid Commun. 27 (2006) 1254–1259. doi:10.1002/marc.200600221.

[33] V. Prosapio, I. De Marco, E. Reverchon, Supercritical antisolvent coprecipitation mechanisms, J. Supercrit. Fluids. 138 (2018) 247–258. doi:10.1016/j.supflu.2018.04.021.

[34] R. Adami, A. Di Capua, E. Reverchon, Supercritical Assisted Atomization for the production of curcumin-biopolymer microspheres, Powder Technol. 305 (2017) 455–461. doi:10.1016/j.powtec.2016.10.020.

[35] D.S. Sogi, S. Sharma, D.P.S. Oberoi, I.A. Wani, Effect of extraction parameters on curcumin yield from turmeric, J. Food Sci. Technol. 47 (2010) 300–304. doi:10.1007/s13197-010-0047-8.

[36] F. Kurniawansyah, R. Mammucari, N.R. Foster, Inhalable curcumin formulations by supercritical technology, Powder Technol. 284 (2015) 289–298. doi:10.1016/j.powtec.2015.04.083.

[37] F. Kurniawansyah, L. Quachie, R. Mammucari, N.R. Foster, Improving the dissolution properties of curcumin using dense gas antisolvent technology, Int. J. Pharm. 521 (2017) 239–248. doi:10.1016/j.ijpharm.2017.02.018.

[38] F. Kurniawansyah, H.T.T. Duong, T.D. Luu, R. Mammucari, O. Vittorio, C. Boyer, N. Foster, Inhalable curcumin formulations: Micronization and bioassay, Chem. Eng. J. 279 (2015) 799–808. doi:10.1016/j.cej.2015.05.087.

[39] K. Chhouk, Wahyudiono, H. Kanda, S.I. Kawasaki, M. Goto, Micronization of curcumin with biodegradable polymer by supercritical anti-solvent using micro swirl mixer, Front. Chem. Sci. Eng. 12 (2018) 184–193. doi:10.1007/s11705-017-1678-3.

[40] W. Wichitnithad, N. Jongaroonngamsang, S. Pummangura, P. Rojsitthisak, A simple isocratic HPLC method for the simultaneous determination of curcuminoids in commercial turmeric extracts, Phytochem. Anal. 20 (2009) 314–319. doi:10.1002/pca.1129.

[41] B. Li, S. Konecke, L.A. Wegiel, L.S. Taylor, K.J. Edgar, Both solubility and chemical stability of curcumin are enhanced by solid dispersion in cellulose derivative matrices, Carbohydr. Polym. 98 (2013) 1108–1116. doi:10.1016/j.carbpol.2013.07.017.

[42] E. Karavas, G. Ktistis, A. Xenakis, E. Georgarakis, Miscibility behavior and formation mechanism of stabilized felodipine-polyvinylpyrrolidone amorphous solid dispersions, Drug Dev. Ind. Pharm. 31 (2005) 473–489. doi:10.1080/03639040500215958.

[43] A. Bouledjouidja, Y. Masmoudi, M. Sergent, V. Trivedi, A. Meniai, E. Badens, Drug loading of foldable commercial intraocular lenses using supercritical impregnation, Int. J. Pharm. 500 (2016) 85–99. doi:10.1016/j.ijpharm.2016.01.016.

[44] J. Li, I.W. Lee, G.H. Shin, X. Chen, H.J. Park, Curcumin-Eudragit® e PO solid dispersion: A simple and potent method to solve the problems of curcumin, Eur. J. Pharm. Biopharm. 94 (2015) 322–332. doi:10.1016/j.ejpb.2015.06.002.

[45] M. Anwar, I. Ahmad, M.H. Warsi, S. Mohapatra, N. Ahmad, S. Akhter, A. Ali, F.J. Ahmad, Experimental investigation and oral bioavailability enhancement of nano-sized curcumin by using supercritical anti-solvent process, Eur. J. Pharm. Biopharm. 96 (2015) 162–172. doi:10.1016/j.ejpb.2015.07.021.

[46] V.J. Pereira, R.L. Matos, S.G. Cardoso, R.O. Soares, G.L. Santana, G.M.N. Costa, S.A.B. Vieira De Melo, A new approach to select solvents and operating conditions for supercritical antisolvent precipitation processes by using solubility parameter and group contribution methods, J. Supercrit. Fluids. 81 (2013) 128–146. doi:10.1016/j.supflu.2013.05.010.

[47] I. Kikic, N. De Zordi, M. Moneghini, D. Solinas, Solubility estimation of drugs in ternary systems of interest for the antisolvent precipitation processes, J. Supercrit. Fluids. 55 (2010) 616–622. doi:10.1016/j.supflu.2010.09.034.

[48] M. Kakran, N.G. Sahoo, I.L. Tan, L. Li, Preparation of nanoparticles of poorly water-soluble antioxidant curcumin by antisolvent precipitation methods, J. Nanoparticle Res. 14 (2012). doi:10.1007/s11051-012-0757-0.

[49] S. Bristow, T. Shekunov, B.Y. Shekunov, P. York, Analysis of the supersaturation and precipitation process with supercritical CO2, J. Supercrit. Fluids. 21 (2001) 257–271. doi:10.1016/S0896-8446(01)00100-0.

[50] A. Martín, M.J. Cocero, Numerical modeling of jet hydrodynamics, mass transfer, and crystallization kinetics in the supercritical antisolvent (SAS) process, J. Supercrit. Fluids. 32 (2004) 203–219. doi:10.1016/j.supflu.2004.02.009.

[51] S.N. Joung, C.W. Yoo, H.Y. Shin, S.Y. Kim, K.P. Yoo, C.S. Lee, W.S. Huh, Measurements and correlation of high-pressure VLE of binary CO2-alcohol systems (methanol, ethanol, 2-methoxyethanol and 2-ethoxyethanol), Fluid Phase Equilib. 185 (2001) 219–230. doi:10.1016/S0378-3812(01)00472-1.

[52] M. Rossmann, A. Braeuer, E. Schluecker, Supercritical antisolvent micronization of PVP and ibuprofen sodium towards tailored solid dispersions, J. Supercrit. Fluids. 89 (2014) 16–27. doi:10.1016/j.supflu.2014.02.010.

[53] A. Gokhale, B. Khusid, R.N. Dave, R. Pfeffer, Effect of solvent strength and operating pressure on the formation of submicrometer polymer particles in supercritical microjets, J. Supercrit. Fluids. 43 (2007) 341–356. doi:10.1016/j.supflu.2007.05.012.

[54] M. Muntó, N. Ventosa, S. Sala, J. Veciana, Solubility behaviors of ibuprofen and naproxen drugs in liquid “CO2-organic solvent” mixtures, J. Supercrit. Fluids. 47 (2008) 147–153. doi:10.1016/j.supflu.2008.07.013.

[55] B. De Gioannis, A. Vega Gonzalez, P. Subra, Anti-solvent and co-solvent effect of CO2 on the solubility of griseofulvin in acetone and ethanol solutions, J. Supercrit. Fluids. 29 (2004) 49–57. doi:10.1016/S0896-8446(03)00035-4.

[56] F. Kurniawansyah, R. Mammucari, N.R. Foster, Polymorphism of curcumin from dense gas

antisolvent precipitation, Powder Technol. 305 (2017) 748–756. doi:10.1016/j.powtec.2016.10.067.

[57] H. Sekikawa, M. Nakano, T. Arita, Inhibitory Effect of Polyvinylpyrrolidone on the Crystallization of Drugs, Chem. Pharm. Bull. 26 (1978) 118–126. doi:10.1248/cpb.26.118.

[58] R.T.Y. Lim, W.K. Ng, R.B.H. Tan, Dissolution enhancement of indomethacin via amorphization using co-milling and supercritical co-precipitation processing, Powder Technol. 240 (2013) 79–87. doi:10.1016/j.powtec.2012.07.004.

[59] F.G. Denardin, S.A.B. Vieira De Melo, R. Mammucari, N.R. Foster, Phase transition and volume expansion in CO2-expanded liquid systems, Chem. Eng. Trans. 32 (2013) 529–534. doi:10.3303/CET1332089.

[60] C.J. Chang, C.-Y. Day, C.-M. Ko, K.-L. Chiu, Densities and P-x-y diagrams for carbon dioxide dissolution in methanol, ethanol, and acetone mixtures, Fluid Phase Equilib. 131 (1997) 243–258.

[61] R. Bos, T. Windono, H.J. Woerdenbag, Y.L. Boersma, A. Koulman, O. Kayser, HPLC-photodiode array detection analysis of curcuminoids in Curcuma species indigenous to Indonesia, Phytochem. Anal. 18 (2007) 118–122. doi:10.1002/pca.959.

[62] G.K. Jayaprakasha, L.J.M. Rao, K.K. Sakariah, Improved HPLC method for the determination of curcumin, demethoxycurcumin, and bisdemethoxycurcumin, J. Agric. Food Chem. 50 (2002) 3668–3672. doi:10.1021/jf025506a.

[63] Y. Long, W. Zhang, F. Wang, Z. Chen, Simultaneous determination of three curcuminoids in Curcuma longa L. by high performance liquid chromatography coupled with electrochemical detection, J. Pharm. Anal. 4 (2014) 325–330. doi:10.1016/j.jpha.2013.10.002.

[64] NIST Chemistry WebBook, Thermophysical Properties of Carbon dioxide, SRD 69. (2017). http://webbook.nist.gov/cgi/fluid.cgi?ID=C124389&Action=Page (accessed January 1, 2017).

[65] D. Bolten, M. Türk, Experimental study on the surface tension, density, and viscosity of

aqueous poly(vinylpyrrolidone) solutions, J. Chem. Eng. Data. 56 (2011) 582–588. doi:10.1021/je101277c.

[66] S.A.B.V. De Melo, L.T. Danh, R. Mammucari, N.R. Foster, Dense CO2 antisolvent precipitation of levothyroxine sodium: A comparative study of GAS and ARISE techniques based on morphology and particle size distributions, J. Supercrit. Fluids. 93 (2014) 112–120. doi:10.1016/j.supflu.2013.11.019.

[67] A. Erriguible, T. Fadli, P. Subra-Paternault, A complete 3D simulation of a crystallization process induced by supercritical CO2to predict particle size, Comput. Chem. Eng. 52 (2013) 1–9. doi:10.1016/j.compchemeng.2012.12.002.

[68] C.S. Lengsfeld, J.P. Delplanque, V.H. Barocas, T.W. Randolph, Mechanism Governing Microparticle Morphology during Precipitation by a Compressed Antisolvent: Atomization vs Nucleation and Growth, J. Phys. Chem. B. 104 (2000) 2725–2735. doi:10.1021/jp9931511.

[69] L.A. Wegiel, Y. Zhao, L.J. Mauer, K.J. Edgar, L.S. Taylor, Curcumin amorphous solid dispersions: the influence of intra and intermolecular bonding on physical stability, Pharm. Dev. Technol. 19 (2014) 976–986. doi:10.3109/10837450.2013.846374.

[70] W.M. Giufrida, R. Favareto, V.F. Cabral, M.A. A.Meireles, L. Cardozo-Filho, M.L. Corazza, High-Pressure Vapor-Liquid Equilibrium Data for Ternary Systems CO2 + Organic Solvent + Curcumin, Open Chem. Eng. J. 4 (2010) 3–10. doi:10.2174/1874123101004020003.

[71] F. Zahran, A. Cabañas, J.A.R. Cheda, J.A.R. Renuncio, C. Pando, Dissolution rate enhancement of the anti-inflammatory drug diflunisal by coprecipitation with a biocompatible polymer using carbon dioxide as a supercritical fluid antisolvent, J. Supercrit. Fluids. 88 (2014) 56–65. doi:10.1016/j.supflu.2014.01.015.

[72] P.R.K. Mohan, G. Sreelakshmi, C. V. Muraleedharan, R. Joseph, Water soluble complexes of curcumin with cyclodextrins: Characterization by FT-Raman spectroscopy, Vib. Spectrosc. 62 (2012) 77–84. doi:10.1016/j.vibspec.2012.05.002.

[73] R.K. Gangwar, V.A. Dhumale, D. Kumari, U.T. Nakate, S.W. Gosavi, R.B. Sharma, S.N.

Kale, S. Datar, Conjugation of curcumin with PVP capped gold nanoparticles for improving bioavailability, Mater. Sci. Eng. C. 32 (2012) 2659–2663. doi:10.1016/j.msec.2012.07.022.

[74] H.A. Garekani, F. Sadeghi, A. Ghazi, Increasing the aqueous solubility of acetaminophen in the presence of polyvinylpyrrolidone and investigation of the mechanisms involved, Drug Dev. Ind. Pharm. 29 (2003) 173–179. doi:10.1081/DDC-120016725.